



Published in final edited form as:

*J Mol Biol.* 2015 May 8; 427(9): 1819–1834. doi:10.1016/j.jmb.2014.12.025.

## Ribosomal initiation complex-driven changes in the stability and dynamics of initiation factor 2 regulate the fidelity of translation initiation

Jiangning Wang, Kelvin Caban, and Ruben L. Gonzalez Jr.

Department of Chemistry, Columbia University, 3000 Broadway, MC3126, New York, NY 10027, USA

### Abstract

Joining of the large, 50S, ribosomal subunit to the small, 30S, ribosomal subunit initiation complex (30S IC) during bacterial translation initiation is catalyzed by initiation factor (IF) 2. Because the rate of subunit joining is coupled to the IF-, transfer RNA (tRNA)-, and messenger RNA (mRNA) codon composition of the 30S IC, the subunit joining reaction functions as a kinetic checkpoint that regulates the fidelity of translation initiation. Recent structural studies suggest that the conformational dynamics of the IF2•tRNA sub-complex that forms on the intersubunit surface of the 30S IC may play a significant role in the mechanisms that couple the rate of subunit joining to the IF-, tRNA-, and codon composition of the 30S IC. To test this hypothesis, we have developed a single-molecule fluorescence resonance energy transfer signal between IF2 and tRNA that has enabled us to monitor the conformational dynamics of the IF2•tRNA sub-complex across a series of 30S ICs. Our results demonstrate that 30S ICs that undergo rapid subunit joining display a high affinity for IF2 and an IF2•tRNA sub-complex that primarily samples a single conformation. In contrast, 30S ICs that undergo slower subunit joining exhibit a decreased affinity for IF2 and/or a change in the conformational dynamics of the IF2•tRNA sub-complex. These results strongly suggest that 30S IC-driven changes in the stability of IF2 and the conformational dynamics of the IF2•tRNA sub-complex regulate the efficiency and fidelity of subunit joining during translation initiation.

### Keywords

Translation initiation; smFRET; 30S IC; binding kinetics; conformational dynamics

---

© 2015 Elsevier Ltd. All rights reserved.

To whom correspondence should be addressed: Ruben L. Gonzalez Jr., Department of Chemistry, Columbia University, 3000 Broadway, MC3126, New York, NY 10027, USA, Tel.: (212) 854-1096; Fax: (212) 932-1289; rlg2118@columbia.edu.

**Publisher's Disclaimer:** This is a PDF file of an unedited manuscript that has been accepted for publication. As a service to our customers we are providing this early version of the manuscript. The manuscript will undergo copyediting, typesetting, and review of the resulting proof before it is published in its final citable form. Please note that during the production process errors may be discovered which could affect the content, and all legal disclaimers that apply to the journal pertain.

### AUTHOR CONTRIBUTIONS

J.W. and R.L.G. designed the research; J.W. performed the experiments; J.W., K.C., and R.L.G. analyzed the data; J.W., K.C., and R.L.G. wrote the manuscript; all three authors approved the final manuscript.

## INTRODUCTION

In bacteria, translation initiation proceeds through a multi-step pathway that can be divided into two major stages (Fig. 1a)<sup>1-4</sup>. In the first stage, three essential initiation factors (IFs; IF1, IF2, and IF3), a specialized initiator transfer RNA (N-formylmethionyl-transfer RNA; fMet-tRNA<sup>fMet</sup>), and a small, or 30S, ribosomal subunit assemble into a 30S initiation complex (30S IC) at the start codon (usually AUG) of a messenger RNA (mRNA). In the second stage, a large, or 50S, ribosomal subunit joins to the 30S IC to form an elongation-competent 70S IC. The fidelity of fMet-tRNA<sup>fMet</sup> and start codon selection during this process are essential for ensuring the integrity of gene expression, as mis-initiation using an elongator tRNA or an internal sense codon leads to proteins containing aberrant N-termini or to frame-shifting errors that yield truncated, and possibly mis-folded, proteins<sup>1,5-8</sup>. Extensive genetic, biochemical, and structural studies of translation initiation suggest that the IFs play crucial and highly complementary roles in regulating the fidelity and the efficiency of translation initiation.

During initiation, IF2 functions synergistically with IF1 and IF3 to selectively accelerate the rate of fMet-tRNA<sup>fMet</sup> binding into the start codon-programmed peptidyl-tRNA binding (P) site of the 30S subunit<sup>9</sup>. Subsequently, in a reaction that is regulated by all three IFs, IF2 accelerates the rate of subunit joining to ‘canonical’ 30S ICs carrying an fMet-tRNA<sup>fMet</sup> that is base paired to a cognate start codon within the P site<sup>10,11</sup>. Highlighting the selectivity with which the IFs regulate the subunit joining reaction, ‘pseudo’ 30S ICs carrying either a non-formylated initiator tRNA (Met-tRNA<sup>fMet</sup>) or an elongator tRNA (*e.g.*, Phe-tRNA<sup>Phe</sup>)<sup>10,12</sup> and ‘non-canonical’ 30S ICs formed at a near-cognate start codon (*e.g.*, an AUU codon)<sup>13,14</sup> exhibit a markedly reduced rate of subunit joining relative to canonical 30S ICs. Despite its importance for regulating the efficiency and the fidelity of translation, the mechanism through which IF2 catalyzes subunit joining and how the IFs collaboratively tune the rate of this reaction in a tRNA- and codon-dependent manner remains poorly understood.

Cryogenic electron microscopy (cryo-EM)-based three-dimensional reconstructions of 30S- and 70S ICs have provided key structural insights into the mechanism through which IF2 catalyzes subunit joining<sup>15-18</sup>. 30S IC structures reveal that domain IV of IF2 (using the domain naming conventions introduced by Roll-Mecak and co-workers<sup>19</sup>) interacts with the acceptor stem of fMet-tRNA<sup>fMet</sup> to form an IF2•tRNA sub-complex on the intersubunit surface of the 30S IC (Fig. 1b) that positions fMet-tRNA<sup>fMet</sup> in an intermediate configuration that has been termed the peptidyl/initiator (P/I) tRNA configuration<sup>15,17,18,20</sup>. The conformation of the IF2•tRNA sub-complex in these structures exhibits striking shape complementarity to a groove in the 50S subunit<sup>17,18</sup> and it has been suggested that the extensive interactions that IF2 makes with this groove underlie the ability of IF2 to catalyze subunit joining<sup>15,17</sup>. In addition, the P/I configuration adopted by fMet-tRNA<sup>fMet</sup> is such that it would allow helix 69 in the 23S ribosomal RNA (rRNA) component of the 50S subunit to access helix 44 in the 16S rRNA component of the 30S subunit, enabling formation of intersubunit bridge B2a, an early forming<sup>21</sup> intersubunit bridge that is critical for the IF-dependent formation of the 70S IC<sup>22</sup>. Thus, because the shape complementarity of IF2 and the 50S subunit as well as the access of 23S rRNA helix 69 to 16S rRNA helix 44 will depend on the conformation of the IF2•tRNA sub-complex, it is possible that the rate of

subunit joining can be tuned by changes in the conformation of the IF2•tRNA sub-complex. Consistent with this possibility, both the position of IF2 and, particularly, the P/I configuration of fMet-tRNA<sup>fMet</sup> that was observed in the cryo-EM structure of the 30S IC lacking IF3<sup>17</sup> differ from that seen in the complete 30S IC<sup>18</sup>, suggesting that the conformation of the IF2•tRNA sub-complex is sensitive to the composition of the 30S IC.

Based on the foregoing structural analysis, we hypothesized that IF-, tRNA-, and codon-dependent changes in the conformational dynamics of the IF2•tRNA sub-complex might provide the mechanistic basis for coupling the rate of subunit joining to the IF-, tRNA-, and codon composition of the 30S IC. To investigate this hypothesis, we have developed an intermolecular IF2-tRNA single-molecule fluorescence resonance energy transfer (smFRET) signal and have used it to characterize the conformational dynamics of the IF2•tRNA sub-complex within a series of canonical, pseudo, and non-canonical 30S ICs that exhibit different rates of subunit joining. Our results show that canonical 30S ICs lacking IF3, which have been shown to undergo relatively rapid subunit joining in ensemble kinetic studies, bind IF2 with a relatively high affinity and yield an IF2•tRNA sub-complex that primarily samples a single conformation. On the other hand, 30S ICs that have been shown to undergo slower subunit joining in ensemble kinetic studies, including canonical 30S ICs that contain IF3, pseudo 30S ICs carrying a non-formylated Met-tRNA<sup>fMet</sup> or Phe-tRNA<sup>Phe</sup>, and non-canonical 30S ICs assembled on an AUU near-cognate start codon, exhibit a decreased affinity for IF2 and/or a change in the conformational dynamics of the IF2•tRNA sub-complex. Interpreted within the context of previous structural and biochemical studies, the smFRET results presented here strongly suggest that IF-, tRNA-, and codon-dependent changes in the structure of the 30S IC regulate the efficiency and fidelity of the subunit joining reaction by modulating the stability of IF2 and the conformational dynamics of the IF2•tRNA sub-complex.

## RESULTS

### Development of an intermolecular IF2-tRNA smFRET signal

Bacterial IF2 is comprised of a non-conserved N-terminal region of variable length and a core C-terminal region comprised of four conserved domains of which domain IV directly contacts the fMet-tRNA<sup>fMet</sup> acceptor stem and formyl moiety<sup>15,17,18</sup>. In order to characterize the real-time dynamics of the interaction between domain IV of IF2 and various P site-bound tRNAs within 30S ICs, we developed an IF2-tRNA smFRET signal between a Cyanine 5 (Cy5), FRET acceptor-labeled IF2 variant (IF2(Cy5)) and various Cyanine 3 (Cy3), FRET donor-labeled tRNA variants, including fMet-tRNA(Cy3)<sup>fMet</sup>, non-formylated Met-tRNA(Cy3)<sup>fMet</sup>, and elongator Phe-tRNA(Cy3)<sup>Phe</sup> (Fig. 1b). IF2(Cy5) was constructed using a mutant IF2 variant that was Cy5-labeled at a surface-exposed cysteine residue that was engineered into domain IV (Supplementary Fig. 1). Using a standard, primer extension inhibition, or “toeprinting”,-based IF2 activity assay<sup>23</sup>, we have demonstrated that IF2(Cy5) can select fMet-tRNA<sup>fMet</sup> over elongator tRNAs within the 30S IC in a manner that is indistinguishable from wildtype IF2 (Supplementary Fig. 2). tRNA(Cy3)<sup>fMet</sup> and tRNA(Cy3)<sup>Phe</sup> were constructed using wildtype tRNA<sup>fMet</sup> and tRNA<sup>Phe</sup> that were Cy3-labeled at naturally occurring, chemically unique, post-transcriptionally modified bases

within their central fold, or “elbow,” domains in a manner that has been previously shown to not impair their functions in translation<sup>24</sup>.

Using our highly purified, reconstituted *in vitro* translation system,<sup>25</sup> 30S ICs containing IF2(Cy5) and variants of tRNA(Cy3)<sup>fMet</sup> or tRNA(Cy3)<sup>Phe</sup> were assembled on 5'-biotinylated mRNAs containing either an AUG or an AUU start codon that is followed by a UUU triplet encoding Phe. As previously described<sup>26</sup>, 30S ICs were then tethered to the polyethylene glycol (PEG)/biotinylated-PEG-derivatized surface of a quartz microfluidic flowcell using a biotin-streptavidin-biotin bridge and imaged at single-molecule resolution at a time resolution of 100 msec frame<sup>-1</sup> using a total internal reflection fluorescence (TIRF) microscope. Control experiments demonstrated that >98% of the single tRNA(Cy3) molecules imaged in our experiments were bound to 30S ICs that were specifically tethered to the PEG/biotinylated-PEG-derivatized surface of the flowcell *via* biotin-streptavidin-biotin bridges to their 5'-biotinylated mRNAs (Supplementary Fig. 3). As an additional control, we used a novel, TIRF-based assay to measure the affinity of fMet-tRNA(Cy3)<sup>fMet</sup> and Phe-tRNA(Cy3)<sup>Phe</sup> binding to a series of canonical, pseudo, and non-canonical 30S ICs containing different combinations of the IFs. These experiments showed that the IF composition of the 30S IC and the identity of the codon in the P site modulates the stabilities of fMet-tRNA(Cy3)<sup>fMet</sup> and Phe-tRNA(Cy3)<sup>Phe</sup> binding to surface-tethered 30S ICs in a manner that is consistent with previous biochemical studies<sup>10,27</sup>, thus validating the biochemical activities of our purified IFs and the ability of our surface-tethered 30S IC- and TIRF-based experimental system to report on biochemical events during translation initiation (Supplementary Fig. 4).

### **30S IC<sub>-1/3</sub> exhibits transient binding of IF2 and an IF2•tRNA sub-complex that is conformationally dynamic**

We began our investigation by collecting FRET efficiency ( $E_{\text{FRET}}$ ) *versus* time trajectories on a canonical 30S IC prepared using fMet-tRNA(Cy3)<sup>fMet</sup>, IF2(Cy5), and an mRNA containing an AUG start codon, but lacking IF1 and IF3 (30S IC<sub>-1/3</sub>). Ensemble kinetic studies have shown that the rate of subunit joining to 30S IC<sub>-1/3</sub> is extremely fast relative to the rate of subunit joining to canonical 30S ICs that contain IF3<sup>9</sup>. Initial attempts to collect 30S IC<sub>-1/3</sub>  $E_{\text{FRET}}$  trajectories using an imaging buffer lacking free IF2(Cy5) suggested that IF2 readily dissociates from 30S IC<sub>-1/3</sub> during surface tethering and TIRF imaging. Thus, unless otherwise specified, we supplemented the imaging buffer used in all IF2-tRNA smFRET experiments with 50 nM IF2(Cy5) such that free IF2(Cy5) from the imaging buffer could rebind to 30S ICs from which IF2(Cy5) may have dissociated. Steady-state 30S IC<sub>-1/3</sub>  $E_{\text{FRET}}$  trajectories collected in the presence of free IF2(Cy5) in the imaging buffer exhibited reversible fluctuations between various FRET states that, according to an  $E_{\text{FRET}}$  histogram of the raw  $E_{\text{FRET}}$  trajectories and a subsequent idealization of the raw  $E_{\text{FRET}}$  trajectories using hidden Markov modeling, encompassed a zero FRET state and at least two non-zero FRET states with  $E_{\text{FRET}}$  distributions centered at  $E_{\text{FRET}}$ s of  $0.5 \pm 0.2$  and  $0.8 \pm 0.1$  (hereafter referred to as IF2-tRNA<sub>0.5,c</sub> and IF2-tRNA<sub>0.8,c</sub> where the subscript c denotes that these states are associated with canonical 30S ICs) (Fig. 2a and Supplementary Fig. 5).

Curve fitting-based population decay analyses (Supplementary Fig. 5f) of the idealized 30S IC<sub>-1/3</sub> E<sub>FRET</sub> trajectories obtained as a function of IF2(Cy5) concentration revealed that the rate of transitions between the zero FRET state and the aggregate non-zero FRET state (*i.e.*, the rate of zero→non-zero FRET transitions) increased as a function of increasing IF2(Cy5) concentration, suggesting that zero→non-zero FRET transitions represent a bimolecular association process. In contrast, the rate of non-zero→zero FRET transitions remained constant as the IF2(Cy5) concentration was increased, suggesting that non-zero→zero FRET transitions represent a unimolecular dissociation process (Supplementary Fig. 6). Thus, we conclude that the zero FRET state corresponds to the IF2-free state of the 30S IC, the aggregate non-zero FRET state corresponds to the IF2-bound state of the 30S IC, and the rates of zero→non-zero and non-zero→zero FRET transitions therefore report on the kinetics of IF2 binding to fMet-tRNA<sup>fMet</sup>-containing 30S IC<sub>-1/3</sub>. Given this interpretation, the apparent rate of IF2 association to 30S IC<sub>-1/3</sub> ( $k_{a,app}$ ) is  $13 \pm 1 \mu\text{M}^{-1} \text{s}^{-1}$ , rate of IF2 dissociation from 30S IC<sub>-1/3</sub> ( $k_{d,app}$ ) is  $0.6 \pm 0.2 \text{s}^{-1}$ , and equilibrium dissociation constant for IF2 binding to 30S IC<sub>-1/3</sub> ( $K_{d,app}$ ) is  $50 \pm 20 \text{nM}$  (Table 1), values that are in excellent agreement with the results of a complementary, transition probability matrix-based population decay analysis of the 30S IC<sub>-1/3</sub> E<sub>FRET</sub> trajectories (Supplementary Table 1).

The stability of the IF2-bound state (*i.e.*, the aggregate non-zero FRET state) for the ensemble of single 30S ICs observed can be visualized as a post-synchronized surface contour plot of the time-evolution of population FRET<sup>24</sup>. These surface contour plots were generated by thresholding each raw E<sub>FRET</sub> trajectory using an E<sub>FRET</sub> of 0.2 to identify individual IF2 binding and dissociation events (see Supplementary Fig 5d), post-synchronizing each binding event such that the first time point that crosses the E<sub>FRET</sub> of 0.2 threshold is reassigned to the 1 sec time point on the plot, and then generating a surface contour plot that effectively superimposes all of the post-synchronized binding events at the 1 sec time point. In such plots, the stability of the IF2-bound state can be easily visualized by assessing the length of time that, starting from the 1 sec time point, the IF2•tRNA sub-complex persists in the aggregate non-zero FRET states prior to transitioning to the zero FRET state. Similarly, reversible fluctuations between zero- and nonzero FRET states (*i.e.*, the reversibility of binding) or between two non-zero FRET states (*i.e.*, fluctuations between different conformational states) can be visualized as a transition density plot (TDP) in which the starting E<sub>FRET</sub> value (x-axis) and the final E<sub>FRET</sub> value (y-axis) for each transition identified in the idealized E<sub>FRET</sub> trajectories are plotted as a surface contour plot<sup>28</sup> (see Supplementary Fig 5e).

The observation of reversible fluctuations between IF2-tRNA<sub>0,5,c</sub> and IF2-tRNA<sub>0,8,c</sub>, defining a dynamic IF2-tRNA<sub>0,8,c</sub>⇌IF2-tRNA<sub>0,5,c</sub> conformational equilibrium, demonstrates that the IF2•tRNA sub-complex within 30S IC<sub>-1/3</sub> exists in a dynamic equilibrium between at least two conformational states in which the distance between our labeling positions differ by ~10 Å (assuming a Förster radius of 55 Å for the Cy3-Cy5 FRET donor-acceptor pair<sup>29,30</sup>). The observation that the IF2•tRNA sub-complex within a 30S IC can occupy at least two conformational states is consistent with, and likely reveals the physical basis for, the biphasic behavior that is typically observed in ensemble kinetic studies of IF2 binding to 30S ICs<sup>11,13,31,32</sup>. Within 30S IC<sub>-1/3</sub>, the IF2•tRNA sub-complex

almost exclusively occupies IF2-tRNA<sub>0.8,c</sub>, only rarely and transiently occupying IF2-tRNA<sub>0.5,c</sub> (Fig. 2a and Supplementary Table 2).

### **Addition of IF1 and IF3 to 30S IC<sub>-1/3</sub> modulates the affinity of IF2 and alters the conformational dynamics of the IF2•tRNA sub-complex**

In ensemble kinetic studies of subunit joining, the presence of IF1 on the 30S IC has been shown to marginally increase the rate of IF2-catalyzed subunit joining whereas IF3, when present alone or along with IF1, has been shown to decrease it<sup>9</sup>. To determine the effect that IF1 and/or IF3 exert on the conformational dynamics of the IF2•tRNA sub-complex, we collected  $E_{\text{FRET}}$  trajectories using canonical 30S ICs that were prepared in a manner analogous to 30S IC<sub>-1/3</sub>, but in the presence of either IF1 (30S IC<sub>-3</sub>), IF3 (30S IC<sub>-1</sub>), or IF1 and IF3 (30S IC<sub>C</sub>) (Fig. 2b–d and Table 1). To ensure that surface-tethered 30S ICs were imaged in the presence of bound IF1 and/or IF3, the imaging buffer was supplemented with saturating concentrations (~1  $\mu\text{M}$ ) of each of these factors. Interestingly, when present independently of each other, we discovered that IF1 and IF3 have opposing effects on the affinity of IF2 for the 30S IC, with IF1 increasing the affinity of IF2 to 30S IC<sub>-3</sub> by decreasing  $K_{\text{d,app}}$  by ~2.5-fold relative to 30S IC<sub>-1/3</sub> and IF3 decreasing the affinity of IF2 to 30S IC<sub>-1</sub> by increasing  $K_{\text{d,app}}$  ~12-fold relative to 30S IC<sub>-1/3</sub>. The increased affinity of IF2 for 30S IC<sub>-3</sub> is kinetically driven by a ~3-fold reduction in  $k_{\text{d,app}}$ , indicating that, relative to 30S IC<sub>-1/3</sub>, an IF1-induced structural rearrangement of 30S IC<sub>-3</sub> strengthens IF2's interactions with 30S IC<sub>-3</sub>. In contrast, the decreased affinity of IF2 for 30S IC<sub>-1</sub> is kinetically driven by a ~4-fold decrease in  $k_{\text{a,app}}$  and a ~4-fold increase in  $k_{\text{d,app}}$ . The decrease in  $k_{\text{a,app}}$  suggests that, relative to 30S IC<sub>-1/3</sub>, an IF3-induced structural rearrangement of 30S IC<sub>-1</sub> decreases the number of IF2–30S IC<sub>-1</sub> collisions that lead to productive binding of IF2 to 30S IC<sub>-1</sub>, whereas the increase in  $k_{\text{d,app}}$  suggests that the same IF3-induced rearrangement of 30S IC<sub>-1</sub> weakens the interactions that IF2 makes with 30S IC<sub>-1</sub> even for collisions that result in productive binding. When present simultaneously, however, IF1 and IF3 result in a dramatic increase in the affinity of IF2 for 30S IC<sub>C</sub> that, relative to 30S IC<sub>-1/3</sub>, yields a decrease in  $K_{\text{d,app}}$  of more than ~30-fold. This increased affinity is kinetically driven by a 1.5-fold decrease in  $k_{\text{a,app}}$  and an ~50-fold decrease in  $k_{\text{d,app}}$ . Thus, maximizing the strength of the interactions that IF2 makes with a canonical 30S IC likely requires a structural rearrangement of the 30S IC that is induced by the synergistic action of IF1 and IF3.

Relative to 30S IC<sub>-1/3</sub>, the exceedingly transient binding of IF2 to 30S IC<sub>-1</sub> yielded a large number of  $E_{\text{FRET}}$  trajectories in which one or more of the observed excursions to non-zero FRET states were captured by only a single frame of the camera detector of the TIRF microscope. To minimize the time-averaging of the  $E_{\text{FRET}}$  that can result from excursions to non-zero FRET states that are shorter than the exposure time of a single frame<sup>33–35</sup>, the  $E_{\text{FRET}}$  was calculated using only those  $E_{\text{FRET}}$  trajectories (~16%) in which all of the observed excursions to non-zero FRET states lasted at least three frames. Analysis of these select  $E_{\text{FRET}}$  trajectories results in the identification of a single, non-zero FRET state with an  $E_{\text{FRET}}$  distribution centered at an  $E_{\text{FRET}}$  of  $0.7 \pm 0.1$  (hereafter referred to as IF2-tRNA<sub>0.7,c</sub>). Although the ~0.1 difference between the means of the  $E_{\text{FRET}}$  distributions for IF2-tRNA<sub>0.8,c</sub> and IF2-tRNA<sub>0.7,c</sub> is within the error of our measurement, it is possible that



the slightly lower mean of the  $E_{\text{FRET}}$  distribution arises from an IF3-induced structural rearrangement of 30S  $IC_{-1}$  that results in a small change in the conformation of the IF2•tRNA sub-complex relative to 30S  $IC_{-1/3}$ . Consistent with this possibility, the 12-fold decrease in the affinity of IF2 to 30S  $IC_{-1}$  relative to 30S  $IC_{-1/3}$  strongly suggests that the IF2•tRNA sub-complexes in these two 30S ICs are indeed different.

Relative to 30S  $IC_{-1/3}$ , the longer-lived binding of IF2 to 30S  $IC_{-3}$  and 30S  $IC_C$  yielded reversible fluctuations between at least two non-zero FRET states with  $E_{\text{FRET}}$  distributions that are centered at  $E_{\text{FRET}}$ s consistent with those of IF2-tRNA<sub>0,8,c</sub> and IF2-tRNA<sub>0,5,c</sub> (Fig. 2d, Supplementary Fig. 7b, and Supplementary Table 2). Interestingly, the presence of IF1 in 30S  $IC_{-3}$  preferentially stabilizes IF2-tRNA<sub>0,8,c</sub> in a manner similar to what is observed in 30S  $IC_{-1/3}$ , whereas the simultaneous presence of IF1 and IF3 in 30S  $IC_C$  shifts the IF2-tRNA<sub>0,8,c</sub> ↔ IF2-tRNA<sub>0,5,c</sub> equilibrium towards IF2-tRNA<sub>0,5,c</sub>. Thus, the structural rearrangement of the canonical 30S IC that is induced by the synergistic action of IF1 and IF3 not only maximizes the strength of the interactions that IF2 makes with the 30S IC, but it also modulates the conformational dynamics of the IF2•tRNA sub-complex such that the relative stabilities of the IF2-tRNA<sub>0,5,c</sub> and IF2-tRNA<sub>0,8,c</sub> conformations of the IF2•tRNA sub-complex within the 30S IC are altered.

### **Pseudo 30S ICs exhibit a decreased affinity for IF2 and an altered conformation of the IF2•tRNA sub-complex**

Thus far we have examined the kinetics of IF2 binding and the conformational dynamics of the IF2•tRNA sub-complex on canonical 30S ICs containing fMet-tRNA<sup>fMet</sup>. As noted earlier, however, pseudo 30S ICs containing either non-formylated Met-tRNA<sup>fMet</sup> or an elongator tRNA exhibit a significant reduction in the rate of IF2-catalyzed subunit joining<sup>10,12</sup>. To determine how these tRNAs might influence the affinity of IF2 for the 30S IC and/or the IF2-tRNA<sub>0,8,c</sub> ↔ IF2-tRNA<sub>0,5,c</sub> conformational equilibrium, we collected  $E_{\text{FRET}}$  trajectories for pseudo 30S ICs that were prepared in a manner analogous to 30S  $IC_C$ , but replacing fMet-tRNA(Cy3)<sup>fMet</sup> with either Met-tRNA(Cy3)<sup>fMet</sup> (30S  $IC_{C,\text{Met}}$ ) or Phe-tRNA(Cy3)<sup>Phe</sup> (30S  $IC_{C,\text{Phe}}$ ). Surprisingly, the  $E_{\text{FRET}}$  trajectories collected for these pseudo 30S ICs did not exhibit any detectable excursions to nonzero FRET states, suggesting that, under our experimental conditions, IF2 binds to these 30S ICs either (i) too rarely to be detected within the limits imposed by the rate of Cy3 photobleaching and/or IF3-induced Met-tRNA(Cy3)<sup>fMet</sup> or Phe-tRNA(Cy3)<sup>Phe</sup> dissociation<sup>10</sup> (ii) too transiently to be detected within the time resolution of our TIRF microscope (100 msec per frame); and/or (iii) in a conformation in which the distance between our labeling positions on IF2 and tRNA is too large to result in a detectable  $E_{\text{FRET}}$ .

Given that IF3 is known to perturb the stability of the P-site tRNA<sup>9,10</sup> we attempted to stabilize the P-site tRNA and increase the probability of observing excursions to non-zero FRET states corresponding to the IF2-bound state of the 30S IC by excluding IF3 from the pseudo 30S ICs. As expected, exclusion of IF3 from 30S  $IC_{C,\text{Met}}$  and 30S  $IC_{C,\text{Phe}}$ , generating 30S  $IC_{-3,\text{Met}}$  and 30S  $IC_{-3,\text{Phe}}$ , yielded detectable, albeit rare and exceedingly transient, excursions to nonzero FRET states corresponding to the IF2-bound state of the 30S IC, resulting in  $K_{d,\text{app}}$  values that are 250–350-fold larger than  $K_{d,\text{app}}$  for 30S  $IC_{-3}$  (Fig.

3, Table 1). After correcting for missing IF2 binding events, we determined that these effects are kinetically driven by ~30–60-fold decreases in  $k_{a,app}$  and ~7–8-fold increases in  $k_{d,app}$  for 30S IC<sub>-3,Met</sub> and 30S IC<sub>-3,Phe</sub>, relative to 30S IC<sub>-3</sub>. Here, the large decrease in  $k_{a,app}$  suggests that, relative to the structure of a canonical 30S IC<sub>-3</sub> carrying fMet-tRNA<sup>fMet</sup>, the structures of the pseudo 30S IC<sub>-3,Met</sub> carrying Met-tRNA<sup>fMet</sup> and the pseudo 30S IC<sub>-3,Phe</sub> carrying Phe-tRNA<sup>Phe</sup> are such that the number of IF2-30S IC collisions that lead to productive binding of IF2 to these pseudo 30S ICs is greatly decreased. Moreover, the increase in  $k_{d,app}$  suggests that the same structures of these pseudo 30S ICs result in a weakening of the interactions that IF2 makes with these pseudo 30S ICs even for collisions that result in productive binding. Indeed, it is likely that the structures of these pseudo 30S ICs are such that the strength of the interactions that domain IV of IF2 makes with Met-tRNA<sup>fMet</sup> or Phe-tRNA<sup>Phe</sup> in 30S IC<sub>-3,Met</sub> and 30S IC<sub>-3,Phe</sub>, respectively, are greatly weakened relative to the interactions that domain IV of IF2 makes with fMet-tRNA<sup>fMet</sup> in 30S IC<sub>-3</sub>.

Consistent with the structural interpretation presented in the previous paragraph, the exceedingly transient binding of IF2 to 30S IC<sub>-3,Met</sub> and 30S IC<sub>-3,Phe</sub> results in broad E<sub>FRET</sub> distributions of non-zero FRET states that are sampled with E<sub>FRET</sub>s in the range of 0.2–1.0 but lacking any distinct peak(s). The broad E<sub>FRET</sub> distributions lacking any distinct peak(s) indicates that the IF2 and tRNA components of the IF2•tRNA sub-complexes that are formed within pseudo 30S ICs can sample a wide range of relative positions, but fail to adopt a well-defined, thermodynamically stable conformation. It is unlikely that our inability to observe any distinct peak(s) in the E<sub>FRET</sub> distributions arises from the time-averaging of E<sub>FRET</sub>s that can result from excursions to non-zero FRET states that are shorter than the exposure time of a single frame<sup>33–35</sup>, as the same broad E<sub>FRET</sub> distribution lacking any distinct peak(s) is observed even when E<sub>FRET</sub>s were calculated using only those E<sub>FRET</sub> trajectories in which all of the observed excursions to non-zero FRET states lasted at least three frames. We note that, in the case of 30S IC<sub>-3,Phe</sub>, the three-nucleotide increase in the length of the spacer between the SD and the UUU codon may contribute to the defect in IF2 binding and the altered E<sub>FRET</sub> distribution. However, the strong similarity between the results obtained with 30S IC<sub>-3,Met</sub> and 30S IC<sub>-3,Phe</sub> (compare Fig 3a and 3b and the corresponding entries in Table 1) strongly argue that these results arise principally from the lack of an fMet-tRNA<sup>fMet</sup> at the P site of these pseudo 30S ICs.

### **Non-canonical 30S ICs exhibit a decreased affinity for IF2 and an altered conformation of the IF2•tRNA sub-complex**

IF3 plays a central role in start-codon recognition<sup>13,14,26,27,36–39</sup> and, in collaboration with IF1, has been shown to regulate the rate of subunit joining in a codon-dependent manner. Indeed, when present simultaneously, IF1 and IF3 significantly reduce the rate of subunit joining to a non-canonical 30S IC assembled on an AUU near-cognate start codon relative to a canonical 30S IC assembled on an AUG start codon<sup>13,14</sup>. When either IF1 or IF3 is excluded from the 30S IC, however, the rate of subunit joining to the non-canonical 30S IC approximates that which is observed for the canonical 30S IC. To explore the possibility that IF1 and IF3 impart codon-dependence to the rate of subunit joining by modulating the stability of IF2 within the 30S IC and/or by altering the conformational dynamics of the



IF2•tRNA sub-complex, we collected  $E_{\text{FRET}}$  trajectories for a series of 30S ICs that were prepared in a manner analogous to that of 30S IC<sub>-1/3</sub>, 30S IC<sub>-3</sub>, 30S IC<sub>-1</sub> and 30S IC<sub>C</sub>, with the exception that they were assembled on an mRNA containing an AUU near-cognate start codon instead of a cognate AUG start codon (30S IC<sub>-1/3,AUU</sub>, 30S IC<sub>-3,AUU</sub>, 30S IC<sub>-1,AUU</sub>, and 30S IC<sub>C,AUU</sub>, respectively) (Fig. 4, Supplementary Fig. 8b–c, and Table 1).

The results of these experiments show that the  $K_{\text{d,app}}$ s, the  $E_{\text{FRET}}$  distributions, and the conformational dynamics of the IF2•tRNA sub-complex observed for 30S IC<sub>-1/3,AUU</sub>, 30S IC<sub>-3,AUU</sub>, and 30S IC<sub>-1,AUU</sub> were almost indistinguishable from those of the corresponding 30S ICs assembled at the AUG codon (compare Fig. 4b and Supplementary Fig. 8b–c with Fig. 2a–c as well as the corresponding entries in Table 1). In contrast,  $K_{\text{d,app}}$  for 30S IC<sub>C,AUU</sub> increases by ~100-fold relative to 30S IC<sub>C</sub>. This decrease in the affinity of IF2 for 30S IC<sub>C,AUU</sub> is kinetically driven by an ~50-fold increase in  $k_{\text{d,app}}$ , indicating that, relative to 30S IC<sub>C</sub>, the structure of the non-canonical 30S IC<sub>C,AUU</sub> programmed with an AUU near-cognate start codon is such that the strength of the interactions that IF2 makes with 30S IC<sub>C,AUU</sub> are greatly reduced.

In addition to the increased  $K_{\text{d,app}}$  and  $k_{\text{d,app}}$ , the transient binding of IF2 to 30S IC<sub>C,AUU</sub> results in sampling of non-zero FRET states (Supplementary Fig. 9) with  $E_{\text{FRET}}$  distributions centered at  $E_{\text{FRET}}$ s of  $0.4 \pm 0.3$  and  $0.7 \pm 0.1$  (hereafter referred to as IF2-tRNA<sub>0.4,nc</sub> and IF2-tRNA<sub>0.7,nc</sub>, where the nc subscript denotes that these states are associated with non-canonical 30S ICs). Relative to IF2-tRNA<sub>0.5,c</sub> and IF2-tRNA<sub>0.8,c</sub>, the means of the distributions for IF2-tRNA<sub>0.4,nc</sub> and IF2-tRNA<sub>0.7,nc</sub> are reduced and, at least in the case of, IF2-tRNA<sub>0.4,nc</sub>, the distributions are broadened. Within 30S IC<sub>C,AUU</sub>, the IF2•tRNA sub-complex only rarely and transiently samples IF2-tRNA<sub>0.4,nc</sub>, almost exclusively occupying IF2-tRNA<sub>0.7,nc</sub> (Fig. 4a and Supplementary Fig. 9). This is in stark contrast to what we observe and described earlier for the corresponding canonical 30S IC (30S IC<sub>C</sub>), which exhibits more frequent and stable excursions between IF2-tRNA<sub>0.5,c</sub> and IF2-tRNA<sub>0.8,c</sub> (compare the transition density plots in Fig. 2d and Fig. 4a). In the case of IF2-tRNA<sub>0.7,nc</sub>, it is unlikely that the reduced mean of the  $E_{\text{FRET}}$  distribution, relative to IF2-tRNA<sub>0.8,c</sub>, arises from the time-averaging of  $E_{\text{FRET}}$ s that can result from excursions to non-zero FRET states that are shorter than the exposure time of a single frame<sup>33–35</sup>, as essentially the same  $E_{\text{FRET}}$  distribution is observed even when  $E_{\text{FRET}}$ s were calculated using only those  $E_{\text{FRET}}$  trajectories in which all of the observed excursions to non-zero FRET states lasted at least three frames. Thus, it is more likely that the reduced mean of the  $E_{\text{FRET}}$  distribution in 30S IC<sub>C,AUU</sub> relative to 30S IC<sub>C</sub> instead arises from a codon-dependent difference between the conformation of the IF2•tRNA sub-complex within 30S IC<sub>C,AUU</sub> and 30S IC<sub>C</sub>. Although the ~0.1 differences between the means of the  $E_{\text{FRET}}$  distributions for IF2-tRNA<sub>0.5,c</sub> and IF2-tRNA<sub>0.4,nc</sub> as well as IF2-tRNA<sub>0.8,c</sub> and IF2-tRNA<sub>0.7,nc</sub> are within the error of our measurements, it is possible that these slightly lower means of the  $E_{\text{FRET}}$  distributions arise from differences in the relative positions of domain IV of IF2 and fMet-tRNA<sup>fMet</sup> in 30S IC<sub>C,AUU</sub> relative to 30S IC<sub>C</sub>. Consistent with this possibility, the 100-fold decrease in the affinity of IF2 and the significantly altered frequency and stability of transitions into IF2-tRNA<sub>0.4,nc</sub> relative to IF2-tRNA<sub>0.5,c</sub> that we only observe when

comparing 30S IC<sub>C,AUU</sub> and 30S IC<sub>C</sub> strongly suggest that the IF2•tRNA sub-complexes in these two 30S ICs are indeed different.

## DISCUSSION

Joining of the 50S subunit to the 30S IC serves as a kinetic checkpoint during translation initiation that is regulated in order to maximize the accuracy of fMet-tRNA<sup>fMet</sup> and start codon selection<sup>9,10,12-14</sup>. The rate of subunit joining is also regulated in order to control the translational efficiency of mRNAs that initiate with non-cognate start codons<sup>13,14</sup>. Although significant strides have been made in understanding the structural basis for IF2's subunit joining activity<sup>15-18</sup>, a complete mechanistic description explaining how the rate of the subunit joining reaction is coupled to the IF-, tRNA-, and codon-composition of the 30S IC is currently unavailable. Here, we have examined the possibility that IF-, tRNA-, and codon-dependent changes to the conformational dynamics of the IF2•tRNA sub-complex may contribute to the mechanism that underlies this coupling. The results of our smFRET studies reveal that the stability of IF2 within a 30S IC and/or the conformational dynamics of the resulting IF2•tRNA sub-complex are significantly dependent on the IF-, tRNA-, and codon composition of the 30S IC. As is described in further detail below, interpretation of our results within the context of the available structural and biochemical data strongly suggest that IF-, tRNA-, and codon-dependent changes to the structure of the 30S IC regulate the efficiency and fidelity of subunit joining reaction by modulating the stability of IF2 and the conformational dynamics of the IF2•tRNA sub-complex.

### IF2-tRNA<sub>0.8,c</sub> represents a conformation of the IF2•tRNA sub-complex within canonical 30S ICs that is associated with rapid subunit joining

Ensemble kinetic studies have shown that the rate of subunit joining to canonical 30S ICs that lack IF3 (30S IC<sub>-1/3</sub> and 30S IC<sub>-3</sub>) is fast compared to analogous canonical 30S ICs containing IF3 (30S IC<sub>-1</sub> and 30S IC<sub>C</sub>)<sup>9,10</sup>. The largest difference (~15-fold) in the rate of subunit joining is seen when comparing 30S IC<sub>-3</sub> and 30S IC<sub>C</sub> (Tables 2 and 3). Despite the faster rate of subunit joining, we show here that IF2 binds ~13-fold less tightly to 30S IC<sub>-3</sub> than to 30S IC<sub>C</sub> (Table 1), suggesting that IF2 makes weaker interactions with 30S IC<sub>-3</sub>. These results indicate that rapid subunit joining does not necessarily require that the strength of the interactions that anchor IF2 to the 30S IC be maximized. Notably, given the  $K_{d,app}$ s for IF2 binding to 30S IC<sub>-3</sub> and 30S IC<sub>C</sub> obtained here (Table 1) and the concentrations of IF2 and other 30S IC components used in ensemble kinetic studies of subunit joining to canonical 30S ICs<sup>9,10</sup>, 30S IC<sub>-3</sub> and 30S IC<sub>C</sub> are predicted to have both been >90% saturated with IF2 in the ensemble kinetic studies of subunit joining (Table 2). Collectively, these observations demonstrate that saturation of 30S ICs with IF2 is not sufficient to maximize the rate of subunit joining and suggest that the conformation of the resulting IF2•tRNA sub-complex is an equally important factor.

Consistent with this possibility, our results demonstrate that the conformational dynamics of the IF2•tRNA sub-complex differs across a series of canonical 30S ICs (Fig. 2). The IF2•tRNA sub-complex within the 30S IC exists in a dynamic IF2-tRNA<sub>0.8,c</sub>  $\rightleftharpoons$  IF2-tRNA<sub>0.5,c</sub> conformational equilibrium. Interestingly, relative to 30S ICs that contain IF3,

30S ICs that lack IF3 exhibit a significant shift in the  $\text{IF2-tRNA}_{0.8,c} \rightleftharpoons \text{IF2-tRNA}_{0.5,c}$  equilibrium towards  $\text{IF2-tRNA}_{0.8,c}$ . Thus,  $\text{IF2-tRNA}_{0.8,c}$  is significantly stabilized over  $\text{IF2-tRNA}_{0.5,c}$  in canonical 30S ICs that undergo rapid subunit joining (*i.e.*, 30S  $\text{IC}_{-1/3}$  and 30S  $\text{IC}_{-3}$ ). In contrast, the relatively slower rate of subunit joining that is observed in 30S  $\text{IC}_{-1}$  and 30S  $\text{IC}_C$  may be partly due to the destabilization of  $\text{IF2-tRNA}_{0.8,c}$  (Fig. 2 and Supplementary Table 2). Within 30S  $\text{IC}_C$ , destabilization of  $\text{IF2-tRNA}_{0.8,c}$  arises from a shift in the  $\text{IF2-tRNA}_{0.8,c} \rightleftharpoons \text{IF2-tRNA}_{0.5,c}$  equilibrium towards  $\text{IF2-tRNA}_{0.5,c}$ , while destabilization of  $\text{IF2-tRNA}_{0.8,c}$  in 30S  $\text{IC}_{-1}$  arises from a change in the conformation of the  $\text{IF2}\cdot\text{tRNA}$  sub-complex that results in  $\text{IF2-tRNA}_{0.7,c}$ .

As described in the Introduction, the ability of IF2 to catalyze subunit joining has been attributed to the extensive interactions that 30S IC-bound IF2 can make with a complementarily shaped groove in the 50S subunit<sup>15,17,18</sup> as well as to the ability of the  $\text{IF2}\cdot\text{tRNA}$  sub-complex to facilitate access to the 30S subunit components that comprise intersubunit bridge B2a<sup>17,18</sup>. It is therefore tempting to speculate that the IF3-mediated destabilization of  $\text{IF2-tRNA}_{0.8,c}$  that we observe here modulates the rate of subunit joining by controlling the degree of complementarity between IF2 and the binding groove in the 50S subunit and/or the accessibility that the 50S subunit has for the 30S subunit components of this critical intersubunit bridge during subunit joining<sup>22</sup>. Alternatively, the IF3-mediated destabilization of  $\text{IF2-tRNA}_{0.8,c}$  may be accompanied by additional changes in the conformation of critical 30S IC components that are not reported on by our  $\text{IF2-tRNA}$  smFRET signal, but that nonetheless inhibit the rate of subunit joining. Indeed, using a different smFRET signal between the 30S IC-bound IF2 and the 50S subunit, we have recently shown that IF3 can modulate both the stability of the 70S IC as well as the conformation of IF2 relative to the 50S subunit within the 70S IC that is formed upon subunit joining<sup>40</sup>. Future X-ray crystallographic or cryo-EM studies of 30S- and 70S ICs formed in the presence and absence of IF3 should provide further insight into the structural basis through which conformational changes of the  $\text{IF2}\cdot\text{tRNA}$  sub-complex and/or additional components of the 30S IC modulate the rate of subunit joining.

### **tRNA-dependent differences in the structure of the 30S IC regulate the rate of subunit joining by modulating the stability of IF2 and the dynamics of the $\text{IF2}\cdot\text{tRNA}$ sub-complex**

Ensemble kinetic studies show that pseudo 30S ICs carrying either a non-formylated Met-tRNA<sup>fMet</sup> or a Phe-tRNA<sup>Phe</sup> exhibit a reduced rate of IF2-catalyzed subunit joining relative to analogous, canonical 30S ICs carrying an fMet-tRNA<sup>fMet</sup><sup>10,12</sup>. Here, we have shown that replacing fMet-tRNA<sup>fMet</sup> with Met-tRNA<sup>fMet</sup> or Phe-tRNA<sup>Phe</sup> yields pseudo 30S ICs in which IF2 is substantially destabilized and the conformational dynamics of the  $\text{IF2}\cdot\text{tRNA}$  sub-complex are altered such that  $\text{IF2-tRNA}_{0.8,c}$  is no longer observed (Table 1) (Fig. 3). The scope of the IF2 destabilization observed here is surprising considering that IF2 has been shown to bind relatively stably to the 30S IC even in the absence of tRNA<sup>13,31,41</sup>. Collectively, these results indicate that binding of IF2 to 30S ICs containing a tRNA other than fMet-tRNA<sup>fMet</sup> is actively inhibited either by steric clashes of domain IV of IF2 with the aminoacyl acceptor end of the tRNA and/or by the inability of domain IV of IF2 to form favorable electrostatic interactions with the aminoacyl acceptor end of the tRNA. The latter possibility is intriguing in light of structural modeling of the  $\text{IF2-tRNA}$  interaction in

*Escherichia coli*, which has revealed that domain IV of IF2 has a positively charged cleft in close proximity to the aminoacyl acceptor end of the tRNA and the observation that IF2 can initiate translation with NH<sub>2</sub>-blocked aminoacyl-tRNAs other than fMet-tRNA<sup>fMet42-44</sup>. Alternatively, or additionally, it is possible that formation of a correctly base paired codon-anticodon interaction within the P site induces, or is accompanied by, a conformational change in the 30S IC that remodels IF2's network of interactions such that the stabilization of IF2 becomes more dependent on its specific interaction with fMet-tRNA<sup>fMet</sup>.

The extent to which the stability of IF2 and the conformational dynamics of the IF2•tRNA sub-complex depend on fMet-tRNA<sup>fMet</sup> is likely sensitive to the IF-composition of the 30S IC. Indeed, a pseudo 30S IC lacking IF1 and IF3 (*i.e.*, 30S IC<sub>-1/3, Met</sub>) results in an ~15-fold decrease in the affinity of IF2 for the 30S IC relative to what is observed in the analogous pseudo 30S IC containing IF1 (*i.e.*, 30S IC<sub>-3, Met</sub>) (Table 1, Supplementary Fig. 8a), a result that is consistent with the stabilizing effect that IF1 has on IF2 binding (Figure 2 and Table 1).

It is important to note that, given the  $K_{d,app}$ s reported in Table 1 and the concentrations of IF2 and other 30S IC components that have been used in ensemble kinetic studies of subunit joining to pseudo 30S ICs analogous to those studied here<sup>10,12</sup>, we predict that the pseudo 30S ICs in the ensemble kinetic studies of subunit joining were not saturated with IF2 (Tables 2 and T3). Thus, from the currently available data, it is not possible to distinguish to what extent the decreased rate of subunit joining that is observed in ensemble kinetic studies of subunit joining to pseudo *versus* canonical 30S ICs results from the reduced occupancy of IF2 on the 30S IC or from the altered conformation that the IF2•tRNA sub-complex adopts in the presence of tRNAs other than fMet-tRNA<sup>fMet</sup>. In order to determine the extent to which subunit joining to pseudo 30S ICs is rate-limited by the conformation of the IF2•tRNA sub-complex, it will be important to conduct future ensemble kinetic studies of subunit joining in which high enough concentrations of IF2 have been used to ensure that pseudo 30S ICs are saturated with IF2.

### **IF1- and IF3-induced, codon-dependent differences in the structure of the 30S IC regulate the rate of subunit joining by modulating the stability of IF2 and the dynamics of the IF2•tRNA sub-complex**

Non-canonical 30S ICs assembled on an mRNA containing an AUU near-cognate start codon (30S IC<sub>C,AUU</sub>) exhibit an IF1- and IF3-dependent decrease in the rate of IF2-catalyzed subunit joining<sup>13,14</sup>. Here, we have shown that replacing an AUG cognate start codon in 30S IC<sub>C</sub> with an AUU near-cognate start codon in 30S IC<sub>C,AUU</sub> yields non-canonical 30S ICs in which IF2 is significantly destabilized and the conformational dynamics of the IF2•tRNA sub-complex are altered (compare Fig 2d and 4a and see Table 1). It is likely that the destabilization of IF2 and the change in the conformational dynamics of the IF2•tRNA sub-complex that are observed in 30S IC<sub>C,AUU</sub> originate from the altered position that fMet-tRNA<sup>fMet</sup> occupies within 30S ICs formed on near-cognate start codons, as has recently been proposed<sup>45</sup>. Notably, given the  $K_{d,app}$ s reported in Table 1 and the concentrations of IF2 and the other 30S IC components that have been used in ensemble kinetic studies of subunit joining to non-canonical 30S ICs analogous to those studied

here<sup>14</sup>, we predict that, in the ensemble kinetic studies of subunit joining, the population of IF2-bound non-canonical 30S ICs was decreased by a factor of only two fold relative to the population of the IF2-bound canonical 30S ICs (Table 2 and 3). This modest, two-fold decrease in the population of IF2-bound non-canonical 30S ICs *versus* IF2-bound canonical 30S ICs is insufficient to explain the ~90-fold decrease in the rate of subunit joining to non-canonical *versus* canonical 30S ICs in the ensemble kinetic studies of subunit joining. Thus, we propose that IF1 and IF3 collaboratively exert their fidelity function and discriminate against near-cognate start codons within non-canonical 30S ICs, at least in part, by perturbing the conformational dynamics of the IF2•tRNA sub-complex. Consistent with this interpretation, Grigoriadou, *et al.*<sup>13</sup> have demonstrated that non-canonical 30S ICs formed on AUU near-cognate start codons exhibit a large, 18-fold decrease in the rate of subunit joining even when using saturating concentrations of a thermophilic IF2 variant that is reported to have a higher affinity than *E. coli* IF2 for *E. coli* 30S ICs<sup>46</sup>.

## MATERIALS AND METHODS

### Preparation and purification of translational components

*E. coli* IF1, the  $\gamma$ -isoform of IF2 (referred to as IF2 throughout this work), and IF3 were overexpressed in BL21(DE3) cells and purified as described previously<sup>25</sup>. 5'-biotinylated mRNAs were variants of the mRNA encoding gene product 32 from T4 bacteriophage and were chemically synthesized (Dharmacon, Inc.). Additional information on the mRNAs used in this work can be found in Supplementary Note 1. tRNA<sup>Phe</sup> (Sigma) was aminoacylated using a fractionated *E. coli* S100 cellular extract containing a mixture of aminoacyl-tRNA (aa-tRNA) synthetases following a previously described procedure<sup>25,47</sup>. tRNA<sup>fMet</sup> (MP Biomedical) was aminoacylated and formylated using purified methionyl-tRNA synthetase (prepared as described by Fourmy *et al.*<sup>48</sup>) and methionyl-tRNA formyltransferase (MTF) (prepared as described by Schmitt *et al.*<sup>49</sup>) following previously published protocols<sup>25</sup>. Met-tRNA<sup>fMet</sup> was prepared using the same protocol that was used to prepare fMet-tRNA<sup>fMet</sup> with the exception that the MTF and the 10-formyltetrahydrofolate formylation substrate were not added to the tRNA<sup>fMet</sup> aminoacylation reaction. Aminoacylated/formylated, aminoacylated, and unacylated tRNAs were separated by hydrophobic interaction chromatography (HIC) on a TSKgel Phenyl-5PW HIC column (Tosoh Bioscience) following a previously described protocol<sup>25</sup>.

30S subunits were purified from *E. coli* strain MRE600 using a combination of protocols<sup>50-52</sup>. Briefly, sucrose density gradient ultracentrifugation was used to purify tight-coupled 70S ribosomes from an *E. coli* MRE600 lysate. Tight-coupled 70S ribosomes were subsequently dissociated into 30S and 50S subunits by dialysis against Ribosome Dissociation Buffer (10 mM tris(hydroxymethyl)aminomethane acetate (pH<sub>4°C</sub> = 7.5), 60 mM ammonium chloride, 1 mM magnesium chloride, 0.5 mM ethylenediamine tetraacetic acid, and 6 mM  $\beta$ -mercaptoethanol). The resulting 30S and 50S subunits were separated by sucrose density gradient ultracentrifugation in Ribosome Dissociation Buffer. The sucrose density gradient fractions corresponding to the 30S subunits were collected, placed into centrifuge tubes, and adjusted to 5 mM Mg<sup>2+</sup> using 1 M magnesium acetate. The centrifuge tubes were then filled with Ribosome Dissociation Buffer which had been adjusted to 7.5



mM Mg<sup>2+</sup> with 1 M magnesium chloride and ultracentrifuged to pellet the purified 30S and 50S subunits. The 30S subunit pellets were resuspended in Ribosome Dissociation Buffer, adjusted to 7.5 mM Mg<sup>2+</sup> with 1 M magnesium chloride, and stored at -80 °C until further use.

### Fluorophore labeling of IF2 and tRNAs

Wildtype *E. coli* IF2 has three cysteines at amino acid positions 599, 815, and 861 (note that the IF2 amino acid numbering used throughout this work corresponds to the  $\alpha$  isoform of IF2). Attempts to generate a cysteine-less variant of IF2 resulted in an IF2 mutant that significantly aggregates during purification and that does not exhibit detectable function in a standard, toeprinting-based assay designed to test the ability of IF2 to select fMet-tRNA<sup>fMet</sup> over elongator tRNAs within the 30S IC<sup>23</sup> (data not shown). Using the QuickChange II-E Site-Directed Mutagenesis Kit (Agilent Technologies) and the mutagenic primers 5'-CGCCGAAATTTTGTGCCATCGCAGGCTGTATG-3' and 5'-CATACAGCCTGCGATGGCACAA AATTTCCGGCG-3', we introduced a fourth cysteine *via* a glycine-to-cysteine mutation at amino acid position 810 (G810C). IF2(G810C) was purified and subsequently fluorescence labeled using a thiol-reactive, maleimide-derivatized Cy5 (GE Life Sciences). By systematically testing fluorescence labeling reaction conditions using IF2(G810C) *versus* wildtype IF2 as a control and quantifying the labeling efficiency using the ratio of IF2 and Cy5 concentrations calculated from the ultraviolet absorbance and molar extinction coefficient at 280 nm of IF2 ( $\epsilon_{280\text{ nm}} = 27,390\text{ M}^{-1}\text{cm}^{-1}$ ; calculated using the ProtParam tool on the ExPASy Proteomics Server (<http://ca.expasy.org/tools/protparam.html>)) and the visible absorbance and molar extinction coefficient at 649 nm of Cy5 ( $\epsilon_{649\text{ nm}} = 250,000\text{ M}^{-1}\text{cm}^{-1}$ ; as reported on the Cy5 mono-reactive maleimide product specification sheet from GE Life Sciences), we found that obtaining selective and efficient labeling of C810 *versus* the three wildtype cysteines was principally a matter of optimizing the Cy5:IF2(G810C) ratio. When the Cy5:IF2(G810C) ratio exceeded 15:1, we began to observe labeling of the wildtype cysteines. However, when the Cy5:IF2(G810C) ratio was 10:1, C810 was selectively labeled with a high efficiency (>95%) while an insignificant level (~2%, essentially background levels) of labeling was observed for the wildtype cysteines (Supplementary Fig. 1). The final, optimized labeling procedure was as follows. IF2(G810C) was buffer exchanged into IF2 Labeling Buffer (10 mM tris(hydroxymethyl)amino methane acetate (pH<sub>4</sub> °C = 7.5) and 50 mM potassium chloride) using Micro Bio-Spin 6 gel filtration spin columns (Bio-Rad) and diluted using IF2 Labeling Buffer to a final concentration of 30  $\mu\text{M}$ . Tris(2-carboxyethyl)phosphine hydrochloride (TCEP-HCl) was added to the IF2(G810C) solution to a final concentration of 300  $\mu\text{M}$  and the IF2(G810C)-TCEP-HCl solution was incubated at room temperature for 30 min to completely reduce any disulfide bonds in IF2(G810C). Following this incubation, a 12 mM Cy5 stock solution was prepared immediately before use by dissolving Cy5 mono-reactive maleimide (GE Life Sciences) in anhydrous dimethyl sulfoxide (Sigma) and an appropriate volume of this Cy5 stock solution was immediately added to the IF2(G810C)-TCEP-HCl solution to obtain a final Cy5 concentration of 300  $\mu\text{M}$ . The reaction was mixed thoroughly and incubated overnight at 4 °C. The mixture was then loaded directly onto a Superdex 200 size-exclusion column (GE Life Sciences) that had been pre-equilibrated using IF2 Size-Exclusion Buffer (40 mM tris(hydroxymethyl)amino methane hydrochloride, 80 mM



sodium chloride, 40 mM ammonium chloride, 5 mM magnesium chloride and 2 mM  $\beta$ -mercaptoethanol) in order to separate Cy5-labeled IF2 (IF2(Cy5)) from unreacted Cy5. The final IF2(G810C) labeling efficiency, which was >95%, was quantified using the ratio of IF2 and Cy5 concentrations calculated using the ultraviolet absorbance and molar extinction coefficient at 280 nm of IF2 and the visible absorbance and molar extinction coefficient at 649 nm of Cy5 (Supplementary Fig. 1).

tRNA<sup>fMet</sup> and tRNA<sup>Phe</sup> were fluorescently labeled and purified following previously published protocols<sup>25</sup>. Briefly, Cy3-labeled tRNA<sup>fMet</sup> (tRNA(Cy3)<sup>fMet</sup>) was prepared by reacting maleimide-derivatized Cy3 (GE Life Sciences) with the naturally occurring 4-thiouridine at nucleotide position 8 within tRNA<sup>fMet</sup>. Cy3-labeled tRNA<sup>Phe</sup> (tRNA(Cy3)<sup>Phe</sup>) was prepared by reacting N-hydroxysuccinimidyl ester-derivatized Cy3 (GE Life Sciences) with the 3-(3-amino-3-carboxypropyl)uridine at nucleotide position 47 within tRNA<sup>Phe</sup>. Unreacted Cy3 was removed from the labeling reactions by extensive phenol extraction, the tRNAs were ethanol precipitated, and Cy3-labeled tRNAs were separated from unlabeled tRNAs on a TSKgel Phenyl-5PW HIC column (Tosoh Bioscience) as previously described<sup>25</sup>. Fractions containing Cy3-labeled tRNAs were pooled, buffer exchanged into NanoPure water using Amicon Ultra centrifugal filters, and stored at  $-20^{\circ}\text{C}$ . Since the Cy3-labeled tRNAs had been purified from the unlabeled tRNAs by HIC, the labeling efficiency of the labeled tRNAs prepared in this manner was ~100%.

### Preparation of 30S ICs

30S ICs were prepared by combining final concentrations of 0.6  $\mu\text{M}$  aa-tRNA(Cy3), 0.9  $\mu\text{M}$  IF1 (when present), 0.9  $\mu\text{M}$  IF3 (when present), 1.8  $\mu\text{M}$  5'-biotinylated mRNA, and 0.6  $\mu\text{M}$  purified *E. coli* 30S subunits in a Tris-Polymix Buffer in which the salt concentration has been optimized as previously described<sup>26</sup> (10 mM tris(hydroxymethyl)aminomethane acetate ( $\text{pH}_{25^{\circ}\text{C}} = 7.0$ ), 20 mM potassium chloride, 1 mM ammonium acetate, 0.1 mM calcium acetate, 5mM magnesium acetate, 0.1 mM ethylenediamine tetraacetic acid, 6 mM  $\beta$ -mercaptoethanol, 5 mM putrescine dihydrochloride, 1 mM spermidine free base, and 1 mM GTP) and incubating the reaction mixture at  $37^{\circ}\text{C}$  for 10 min. The 30S IC sample was then transferred directly to ice and incubated for 5 min. Finally, the 30S IC sample was divided into small aliquots that were flash frozen in liquid nitrogen, stored at  $-80^{\circ}\text{C}$ , and thawed and imaged within 24 hours of preparation.

### TIRF microscopy and smFRET experiments

Quartz microfluidic flowcells were passivated using a mixture of polyethyleneglycol (PEG) and biotinylated PEG (biotin-PEG) and were subsequently derivatized with streptavidin immediately before use as previously described<sup>52</sup>. Each 30S IC sample was diluted using Tris-Polymix Buffer such that the final aa-tRNA(Cy3) concentration generated ~300 surface-tethered 30S ICs per field of view (FOV =  $60 \times 120 \mu\text{m}$ ) (Supplementary Table 3). When present in a particular 30S IC sample, unlabeled IFs were added to the dilution buffer at the same concentrations at which they were used to assemble the 30S IC, thus ensuring that the 30S IC was saturated with unlabeled IFs during the dilution. Immediately upon dilution, the 30S IC sample was loaded into the flowcell and incubated for 10 min at room temperature. 30S ICs that were not tethered during the incubation time were removed from

the flowcell by washing the flowcell twice with 50  $\mu\text{L}$  of the corresponding dilution buffer. We note that the total volume of each flowcell was  $\sim 7 \mu\text{L}$ . During the second wash step, the buffer was further supplemented with 50 nM IF2(Cy5), an oxygen-scavenging system (300  $\mu\text{g}/\text{mL}$  glucose oxidase, 40  $\mu\text{g}/\text{mL}$  catalase and 1%  $\beta\text{-D-glucose}$ ), and a triplet-state quencher cocktail (1 mM 1,3,5,7-cyclooctatetraene (Aldrich) and 1 mM *p*-nitrobenzyl alcohol (Fluka)). The time required to wash the flowcell and mount it onto the microscope stage for imaging was standardized to 5 min across all 30S IC samples.

Surface-tethered 30S ICs carrying P site-bound aa-tRNA(Cy3)s were imaged at single-molecule resolution using a previously described<sup>53</sup>, laboratory-built, wide-field, prism-based TIRF microscope. Cy3 fluorophores were directly excited using a 532 nm diode-pumped solid-state laser (CrystaLaser, Inc.) operating at a power of 12 mW (measured just before striking the prism). The Cy3 and, when present, Cy5 emission from each of  $\sim 300$  surface-tethered 30S ICs were collected by a 1.2 numerical aperture 60 $\times$  objective (Nikon), wavelength separated by a Dual-View multichannel imaging system (Photometrics, Inc), and imaged onto a 512  $\times$  512 pixel electron-multiplying charge-coupled device (EMCCD) camera (Cascade II 512:B, Photometrics, Inc.) operating with 2 $\times$ 2 pixel binning at a time resolution of 100 ms frame<sup>-1</sup> for experiments involving continuous laser excitation. Experiments involving shuttering of the laser excitation source were performed by collecting single, 100 ms frames at shuttered time intervals of 0–13 s (Supplementary Fig. 10). 30S ICs were imaged over a long enough observation period (50–100 s) such that the majority of the fluorophores in the FOV were photobleached during the observation period.

### smFRET data analysis

Cy3 and Cy5 emission intensities *versus* time trajectories for each 30S IC were generated using the MetaMorph image analysis software (Molecular Dynamics, Inc) and following slight modifications of previously described protocols<sup>53</sup>. Briefly, the Cy3 and Cy5 halves of each movie were divided into separate Cy3 and Cy5 movies. Single Cy5 fluorophores in each Cy5 movie were distinguished from the background noise by applying an intensity threshold to a single composite image containing the maximum pixel value for each pixel across all frames of the movie. Using the maximum pixel value for each pixel across all frames of the Cy5 movie to identify single Cy5 fluorophores ensured that 30S ICs undergoing even a single IF2(Cy5) binding event at any time during the movie were captured. The Cy3 fluorophore corresponding to each selected Cy5 fluorophore was then identified by aligning the first frame of the Cy3 movie with the single composite image of the corresponding Cy5 movie. This image analysis protocol resulted in the identification of the set of single Cy3-Cy5 FRET pairs for each movie. Cy3 and Cy5 emission intensities *versus* time trajectories were then plotted and only those trajectories in which the Cy3 and Cy5 fluorophores underwent single-step photobleaching during the observation time, or in which the Cy3 and Cy5 fluorophores did not undergo photobleaching during the observation time but nevertheless exhibited anti-correlation and average Cy3 and Cy5 emission intensities that fell within the distribution of emission intensities observed for *bona fide* single Cy3 and Cy5 fluorophores, were used for further analysis. Using custom scripts written in Matlab (MathWorks), the Cy5 emission intensity was corrected for the  $\sim 7\%$  bleedthrough of Cy3 emission intensity into the Cy5 channel and the Cy3 and Cy5 emission

intensities were baseline corrected such that, after photobleaching of Cy3 and Cy5, the Cy3 and Cy5 emission intensities averaged to zero (Supplementary Fig. 5a).  $E_{\text{FRET}}$  versus time trajectories were generated by calculating the value of the  $E_{\text{FRET}}$  at each time point along each Cy3 and Cy5 emission intensities versus time trajectory using  $E_{\text{FRET}} = I_{\text{Cy5}}(I_{\text{Cy5}} + I_{\text{Cy3}})$ , where  $I_{\text{Cy3}}$  and  $I_{\text{Cy5}}$  correspond to the bleedthrough- and baseline-corrected Cy3 and Cy5 emission intensities, respectively (Supplementary Fig. 5a).

$E_{\text{FRET}}$  versus time trajectories were idealized to a hidden Markov model (HMM) using the software program HaMMY<sup>28</sup>. With the exception of 30S IC<sub>C</sub>, 30S IC<sub>-1/3,Met</sub>, 30S IC<sub>-3,Met</sub>, and 30S IC<sub>-3,Phc</sub>,  $k_{\text{a,app}}$ ,  $k_{\text{d,app}}$ , and  $K_{\text{d,app}}$  for the interaction of IF2 with each 30S IC were determined by conducting curve fitting-based population decay analyses of the idealized  $E_{\text{FRET}}$  versus time trajectories obtained from steady-state smFRET experiments recorded using continuous laser excitation in a manner analogous to that which we have previously described<sup>53,54</sup> and that is described in detail in Supplementary Fig. 5f and in Supplementary Notes 3 and 4. 30S IC<sub>C</sub> exhibited stable and long-lived IF2 binding events such that the accuracy with which  $k_{\text{a,app}}$ ,  $k_{\text{d,app}}$ , and  $K_{\text{d,app}}$  can be determined using curve-fitting based population decay analyses of the idealized  $E_{\text{FRET}}$  versus time trajectories obtained from steady-state smFRET experiments recorded using continuous laser excitation becomes limited by the small number of excursions to the zero FRET state that are observed in the  $E_{\text{FRET}}$  trajectories prior to photobleaching of the Cy3 and/or Cy5 fluorophores. Thus,  $k_{\text{a,app}}$ ,  $k_{\text{d,app}}$ , and  $K_{\text{d,app}}$  were determined using a pre-steady-state smFRET experiment and an smFRET experiment in which the laser excitation source was shuttered that is described in detail in Supplementary Fig. 10 and Supplementary Notes 3 and 4. In contrast, 30S IC<sub>-1/3,Met</sub>, 30S IC<sub>-3,Met</sub>, and 30S IC<sub>-3,Phc</sub> exhibited extremely rare and transient IF2 binding events such that the accuracy with which  $k_{\text{a,app}}$  can be calculated using curve fitting-based population decay analyses becomes limited by the small number of excursions to the non-zero FRET state that are observed in the  $E_{\text{FRET}}$  trajectories prior to photobleaching of the Cy3 fluorophore. Thus,  $k_{\text{a,app}}$ ,  $k_{\text{d,app}}$ , and  $K_{\text{d,app}}$  for each of these 30S ICs were determined using a combination of curve fitting-based and transition probability matrix-based population decay analyses as described in detail in Supplementary Table 1 and Supplementary Table in Supplementary Notes 3 and 4.

## Supplementary Material

Refer to Web version on PubMed Central for supplementary material.

## ACKNOWLEDGEMENTS

This work was supported by funds to R.L.G. from the Burroughs Wellcome Fund (CABS 1004856) and the NIH (R01 GM 084288). K.C. was supported by an American Cancer Society Postdoctoral fellowship (125201). We would like to thank Dr. Daniel MacDougall, Dr. Margaret Elvekrog, Mr. Colin Kinz Thompson, and Ms. Bridget Huang for insightful discussions and advice and Mr. Corey Perez for managing the Gonzalez laboratory.

## ABBREVIATIONS

**IF** Initiation factor

<b>IC</b>	initiation complex
<b>smFRET</b>	single-molecule fluorescence resonance energy transfer
<b>TIRF</b>	total internal reflection microscopy
<b>tRNA</b>	transfer ribonucleic acid
<b>rRNA</b>	ribosomal ribonucleic acid
<b>Phe</b>	phenylalanine
<b>fMet</b>	N-formylated methionine
<b>cryo-EM</b>	cryogenic electron microscopy
<b>Cy</b>	cyanine
<b>PEG</b>	polyethylene glycol
<b>E<sub>FRET</sub></b>	FRET efficiency
<b><math>k_{a,app}</math></b>	apparent association rate constant
<b><math>k_{d,app}</math></b>	apparent dissociation rate constant
<b><math>K_{d,app}</math></b>	apparent equilibrium dissociation constant
<b>P-site</b>	peptidyl site
<b>EMCCD</b>	electron-multiplying charge-coupled-device
<b><i>I</i></b>	Intensity

## REFERENCES

1. Laursen BS, Sørensen HP, Mortensen KK, Sperling-Petersen HU. Initiation of protein synthesis in bacteria. *Microbiol Mol Biol Rev.* 2005; 69:101–123. [PubMed: 15755955]
2. Simonetti A, Marzi S, Jenner L, Myasnikov A, Romby P, Yusupova G, Klaholz BP, Yusupov M. A structural view of translation initiation in bacteria. *Cell Mol Life Sci.* 2009; 66:423–436. [PubMed: 19011758]
3. Gualerzi C, Fabbretti A, Brandi L, Milon P, Pon C. Role of the Initiation Factors in mRNA Start Site Selection and fMet-tRNA Recruitment by Bacterial Ribosomes. *Israel Journal of Chemistry.* 2010; 50:80–94.
4. Milón P, Rodnina MV. Kinetic control of translation initiation in bacteria. *Crit Rev Biochem Mol Biol.* 2012; 47:334–348. [PubMed: 22515367]
5. Farabaugh PJ, Björk GR. How translational accuracy influences reading frame maintenance. *EMBO J.* 1999; 18:1427–1434. [PubMed: 10075915]
6. Clemens MJ, Bommer UA. Translational control: the cancer connection. *Int J Biochem Cell Biol.* 1999; 31:1–23. [PubMed: 10216939]
7. Farabaugh PJ. Translational frameshifting: implications for the mechanism of translational frame maintenance. *Prog Nucleic Acid Res Mol Biol.* 2000; 64:131–170. [PubMed: 10697409]
8. Watkins SJ, Norbury CJ. Translation initiation and its deregulation during tumorigenesis. *Br J Cancer.* 2002; 86:1023–1027. [PubMed: 11953842]
9. Antoun A, Pavlov MY, Lovmar M, Ehrenberg M. How initiation factors tune the rate of initiation of protein synthesis in bacteria. *EMBO J.* 2006; 25:2539–2550. [PubMed: 16724118]

10. Antoun A, Pavlov MY, Lovmar M, Ehrenberg M. How initiation factors maximize the accuracy of tRNA selection in initiation of bacterial protein synthesis. *Mol Cell*. 2006; 23:183–193. [PubMed: 16857585]
11. Grigoriadou C, Marzi S, Kirillov S, Gualerzi CO, Cooperman BS. A quantitative kinetic scheme for 70 S translation initiation complex formation. *J Mol Biol*. 2007; 373:562–572. [PubMed: 17868692]
12. Pavlov MY, Zorzet A, Andersson DI, Ehrenberg M. Activation of initiation factor 2 by ligands and mutations for rapid docking of ribosomal subunits. *EMBO J*. 2011; 30:289–301. [PubMed: 21151095]
13. Grigoriadou C, Marzi S, Pan D, Gualerzi CO, Cooperman BS. The translational fidelity function of IF3 during transition from the 30 S initiation complex to the 70 S initiation complex. *J Mol Biol*. 2007; 373:551–561. [PubMed: 17868695]
14. Milon P, Konevega AL, Gualerzi CO, Rodnina MV. Kinetic checkpoint at a late step in translation initiation. *Mol Cell*. 2008; 30:712–720. [PubMed: 18570874]
15. Allen GS, Zavialov A, Gursky R, Ehrenberg M, Frank J. The cryo-EM structure of a translation initiation complex from *Escherichia coli*. *Cell*. 2005; 121:703–712. [PubMed: 15935757]
16. Myasnikov AG, Marzi S, Simonetti A, Giuliodori AM, Gualerzi CO, Yusupova G, Yusupov M, Klaholz BP. Conformational transition of initiation factor 2 from the GTP- to GDP-bound state visualized on the ribosome. *Nat Struct Mol Biol*. 2005; 12:1145–1149. [PubMed: 16284619]
17. Simonetti A, Marzi S, Myasnikov AG, Fabbretti A, Yusupov M, Gualerzi CO, Klaholz BP. Structure of the 30S translation initiation complex. *Nature*. 2008; 455:416–420. [PubMed: 18758445]
18. Julián P, Milon P, Agirrezabala X, Lasso G, Gil D, Rodnina MV, Valle M. The Cryo-EM structure of a complete 30S translation initiation complex from *Escherichia coli*. *PLoS Biol*. 2011; 9:e1001095. [PubMed: 21750663]
19. Roll-Mecak A, Cao C, Dever TE, Burley SK. X-Ray structures of the universal translation initiation factor IF2/eIF5B: conformational changes on GDP and GTP binding. *Cell*. 2000; 103:781–792. [PubMed: 11114334]
20. Graifer DM, Babkina GT, Matasova NB, Vladimirov SN, Karpova GG, Vlassov VV. Structural arrangement of tRNA binding sites on *Escherichia coli* ribosomes, as revealed from data on affinity labelling with photoactivatable tRNA derivatives. *Biochimica et Biophysica Acta (BBA) - Gene Structure and Expression*. 1989; 1008:146–156.
21. Hennelly SP, Antoun A, Ehrenberg M, Gualerzi CO, Knight W, Lodmell JS, Hill WE. A time-resolved investigation of ribosomal subunit association. *J Mol Biol*. 2005; 346:1243–1258. [PubMed: 15713478]
22. Kipper K, Hetényi C, Sild S, Remme J, Liiv A. Ribosomal intersubunit bridge B2a is involved in factor-dependent translation initiation and translational processivity. *J Mol Biol*. 2009; 385:405–422. [PubMed: 19007789]
23. Hartz D, McPheeters DS, Gold L. Selection of the initiator tRNA by *Escherichia coli* initiation factors. *Genes Dev*. 1989; 3:1899–1912. [PubMed: 2695390]
24. Blanchard SC, Gonzalez RL, Kim HD, Chu S, Puglisi JD. tRNA selection and kinetic proofreading in translation. *Nat Struct Mol Biol*. 2004; 11:1008–1014. [PubMed: 15448679]
25. Fei J, Wang J, Sternberg SH, MacDougall DD, Elvekrog MM, Pulukkunat DK, Englander MT, Gonzalez RL. A highly purified, fluorescently labeled in vitro translation system for single-molecule studies of protein synthesis. *Methods Enzymol*. 2010; 472:221–259. [PubMed: 20580967]
26. Elvekrog MM, Gonzalez RL. Conformational selection of translation initiation factor 3 signals proper substrate selection. *Nat Struct Mol Biol*. 2013; 20:628–633. [PubMed: 23584454]
27. La Teana A, Pon CL, Gualerzi CO. Translation of mRNAs with degenerate initiation triplet AUU displays high initiation factor 2 dependence and is subject to initiation factor 3 repression. *Proc Natl Acad Sci U S A*. 1993; 90:4161–4165. [PubMed: 8483930]
28. McKinney SA, Joo C, Ha T. Analysis of single-molecule FRET trajectories using hidden Markov modeling. *Biophys J*. 2006; 91:1941–1951. [PubMed: 16766620]

29. Bastiaens PI, Jovin TM. Microspectroscopic imaging tracks the intracellular processing of a signal transduction protein: fluorescent-labeled protein kinase C beta I. *Proc Natl Acad Sci U S A*. 1996; 93:8407–8412. [PubMed: 8710884]
30. Hohng S, Joo C, Ha T. Single-molecule three-color FRET. *Biophys J*. 2004; 87:1328–1337. [PubMed: 15298935]
31. Milon P, Carotti M, Konevega AL, Wintermeyer W, Rodnina MV, Gualerzi CO. The ribosome-bound initiation factor 2 recruits initiator tRNA to the 30S initiation complex. *EMBO Rep*. 2010; 11:312–316. [PubMed: 20224578]
32. Milón P, Maracci C, Filonava L, Gualerzi CO, Rodnina MV. Real-time assembly landscape of bacterial 30S translation initiation complex. *Nat Struct Mol Biol*. 2012; 19:609–615. [PubMed: 22562136]
33. Bronson JE, Fei J, Hofman JM, Gonzalez RL, Wiggins CH. Learning rates and states from biophysical time series: a Bayesian approach to model selection and single-molecule FRET data. *Biophys J*. 2009; 97:3196–3205. [PubMed: 20006957]
34. van de Meent JW, Bronson JE, Wiggins CH, Gonzalez RL. Empirical Bayes methods enable advanced population-level analyses of single-molecule FRET experiments. *Biophys J*. 2014; 106:1327–1337. [PubMed: 24655508]
35. Kinz-Thompson CD, Gonzalez RL. smFRET studies of the ‘encounter’ complexes and subsequent intermediate states that regulate the selectivity of ligand binding. *FEBS Lett*. 2014
36. Butler J, Springer M, Dondon J, Graffe M, Grunberg-Manago M. Escherichia coli protein synthesis initiation factor IF3 controls its own gene expression at the translational level in vivo. *Journal of Molecular Biology*. 1986; 192:767–780. [PubMed: 2438418]
37. Butler JS, Springer M, Grunberg-Manago M. AUU-to-AUG mutation in the initiator codon of the translation initiation factor IF3 abolishes translational autocontrol of its own gene (infC) in vivo. *Proc Natl Acad Sci U S A*. 1987; 84:4022–4025. [PubMed: 2954162]
38. Hartz D, Binkley J, Hollingsworth T, Gold L. Domains of initiator tRNA and initiation codon crucial for initiator tRNA selection by Escherichia coli IF3. *Genes Dev*. 1990; 4:1790–1800. [PubMed: 1701151]
39. Meinnel T, Sacerdot C, Graffe M, Blanquet S, Springer M. Discrimination by Escherichia coli initiation factor IF3 against initiation on non-canonical codons relies on complementarity rules. *Journal of Molecular Biology*. 1999; 290:825–837. [PubMed: 10398584]
40. MacDougall DD, Gonzalez RL. Translation initiation factor 3 regulates switching between different modes of ribosomal subunit joining. *J Mol Biol*. 2014
41. Weil J, Hershey JW. The binding of fluorescein-labeled protein synthesis initiation factor 2 to Escherichia coli 30 S ribosomal subunits determined by fluorescence polarization. *J Biol Chem*. 1982; 257:1215–1220. [PubMed: 6799502]
42. Wintermeyer W, Gualerzi C. Effect of Escherichia coli initiation factors on the kinetics of N-Acph-tRNA<sup>Phe</sup> binding to 30S ribosomal subunits. A fluorescence stopped-flow study. *Biochemistry*. 1983; 22:690–694. [PubMed: 6340723]
43. Gualerzi CO, Wintermeyer W. Prokaryotic initiation factor 2 acts at the level of the 30 S ribosomal subunit: a fluorescence stopped-flow study. *FEBS letters*. 1986; 202:1–6.
44. Steiner-Mosonyi M, Creuzenet C, Keates RA, Strub BR, Mangroo D. The Pseudomonas aeruginosa initiation factor IF-2 is responsible for formylation-independent protein initiation in P. aeruginosa. *J Biol Chem*. 2004; 279:52262–52269. [PubMed: 15385567]
45. Qin D, Liu Q, Devaraj A, Fredrick K. Role of helix 44 of 16S rRNA in the fidelity of translation initiation. *RNA*. 2012; 18:485–495. [PubMed: 22279149]
46. Qin H, Grigoriadou C, Cooperman BS. Interaction of IF2 with the ribosomal GTPase-associated center during 70S initiation complex formation. *Biochemistry*. 2009; 48:4699–4706. [PubMed: 19366171]
47. Carbon J, David H. Studies on the thionucleotides in transfer ribonucleic acid. Addition of N-ethylmaleimide and formation of mixed disulfides with thiol compounds. *Biochemistry*. 1968; 7:3851–3858. [PubMed: 4881059]



48. Fourmy D, Mechulam Y, Brunie S, Blanquet S, Fayat G. Identification of residues involved in the binding of methionine by Escherichia coli methionyl-tRNA synthetase. *FEBS Lett.* 1991; 292:259–263. [PubMed: 1959615]
49. Schmitt E, Blanquet S, Mechulam Y. Crystallization and preliminary X-ray analysis of Escherichia coli methionyl-tRNAMet(f) formyltransferase complexed with formyl-methionyl-tRNAMet(f). *Acta Crystallogr D Biol Crystallogr.* 1999; 55:332–334. [PubMed: 10089442]
50. Paulsen H, Robertson JM, Wintermeyer W. Effect of ribosome binding and translocation on the anticodon of tRNAPhe as studied by wybutine fluorescence. *Nucleic Acids Res.* 1982; 10:2651–2663. [PubMed: 7043399]
51. Powers T, Noller HF. A functional pseudoknot in 16S ribosomal RNA. *EMBO J.* 1991; 10:2203–2214. [PubMed: 1712293]
52. Blanchard SC, Kim HD, Gonzalez RL, Puglisi JD, Chu S. tRNA dynamics on the ribosome during translation. *Proc Natl Acad Sci U S A.* 2004; 101:12893–12898. [PubMed: 15317937]
53. Fei J, Kosuri P, MacDougall DD, Gonzalez RL. Coupling of ribosomal L1 stalk and tRNA dynamics during translation elongation. *Mol Cell.* 2008; 30:348–359. [PubMed: 18471980]
54. Fei J, Bronson JE, Hofman JM, Srinivas RL, Wiggins CH, Gonzalez RL. Allosteric collaboration between elongation factor G and the ribosomal L1 stalk directs tRNA movements during translation. *Proc Natl Acad Sci U S A.* 2009; 106:15702–15707. [PubMed: 19717422]
55. Copeland, RA. *Enzymes a practical introduction to structure, mechanism, and data analysis.* New York: Wiley; 2000. p. 76-108.

### Highlights

Initiation factor 2 (IF2) catalyzes ribosomal 50S subunit joining to the ribosomal 30S initiation complex (30S IC) through the formation of a 30S IC-bound IF2•tRNA subcomplex.

We have developed a novel IF2-tRNA single-molecule fluorescence resonance energy transfer (smFRET) signal to monitor the stability and dynamics of the IF2•tRNA subcomplex on the 30S IC.

We show that IF2 binds stably to 30S ICs that are associated with rapid subunit joining and that the IF2•tRNA sub-complex in these 30S ICs favors a single conformation.

Additionally, we show that IF2 binds either less stably to, or forms an IF2•tRNA subcomplex with altered dynamics on, 30S ICs associated with slower subunit joining.

We conclude that the stability of IF2 and the conformational dynamics of the IF2•tRNA sub-complex can be tuned in order to regulate the rate of subunit joining.

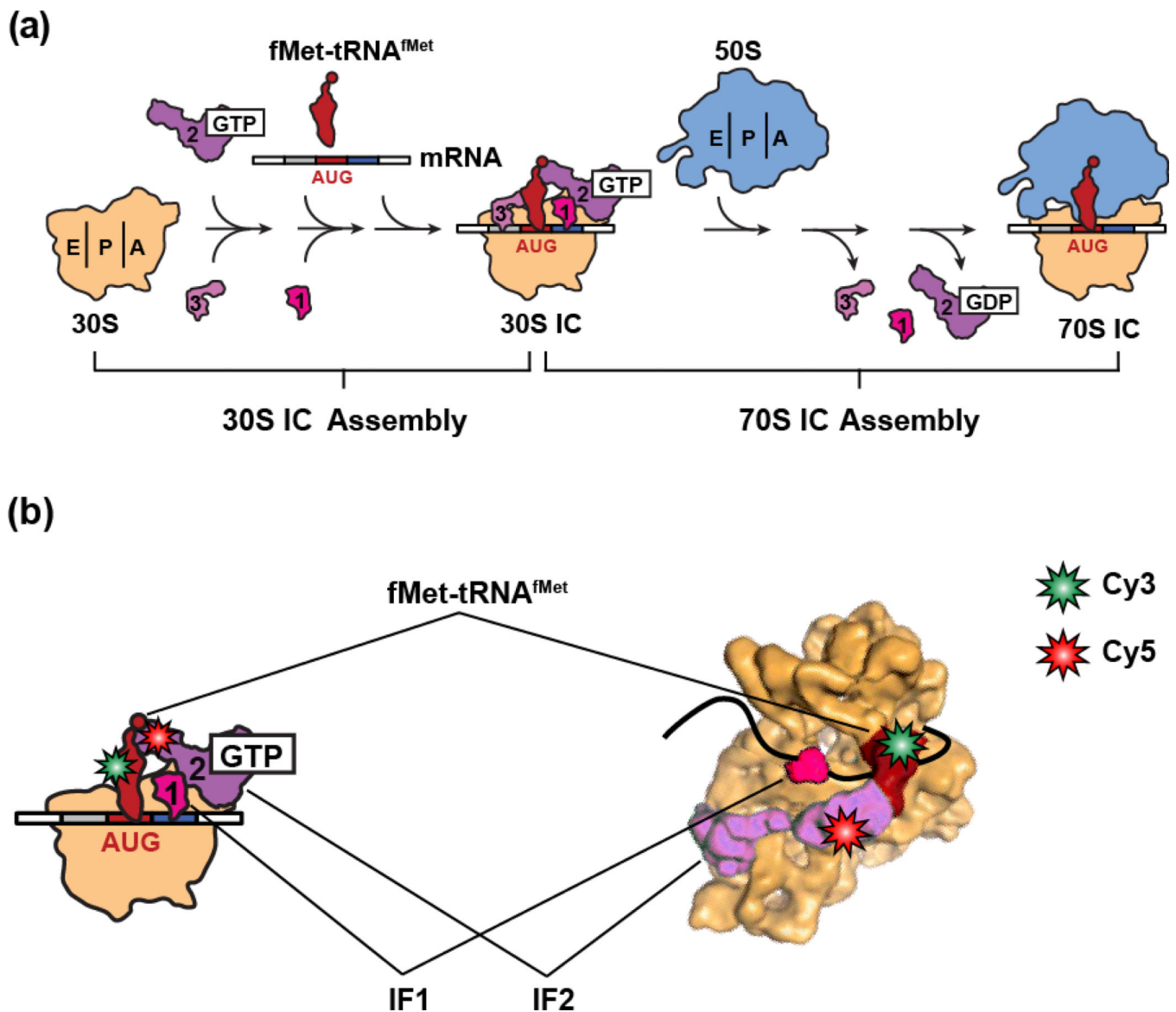


**Figure 1.**

(a) Cartoon representation of the canonical translation initiation pathway. During the first major step of translation initiation, the IFs bind to the 30S subunit and collaboratively increase the rate and accuracy of fMet-tRNA<sup>fMet</sup> selection and decoding of the start codon within the P site of the 30S subunit, resulting in the assembly of a 30S IC at the start codon of the mRNA to be translated. During the second major step, the 50S subunit joins to the 30S IC, the IFs are released from the resulting 70S IC, and fMet-tRNA<sup>fMet</sup> is positioned into the peptidyl transferase center of the 50S subunit, resulting in the assembly of an elongation-competent 70S IC. (b) A cartoon representation (left panel) and cryogenic electron microscopy (cryo-EM) structural model (right panel) depicting the IF2-tRNA smFRET signal used to monitor the conformational dynamics of the IF2-tRNA sub-complex within 30S ICs. IF2 was labeled with a Cy5 FRET acceptor at a cysteine residue that was engineered into domain IV of IF2 and fMet-tRNA<sup>fMet</sup> or variants thereof were labeled with

a Cy3 FRET donor within their central fold, or “elbow”, domains. The figure depicting the cryo-EM structural model was adapted from a figure published in Simonetti et al., 2008<sup>17</sup>.

Author Manuscript

Author Manuscript

Author Manuscript

Author Manuscript

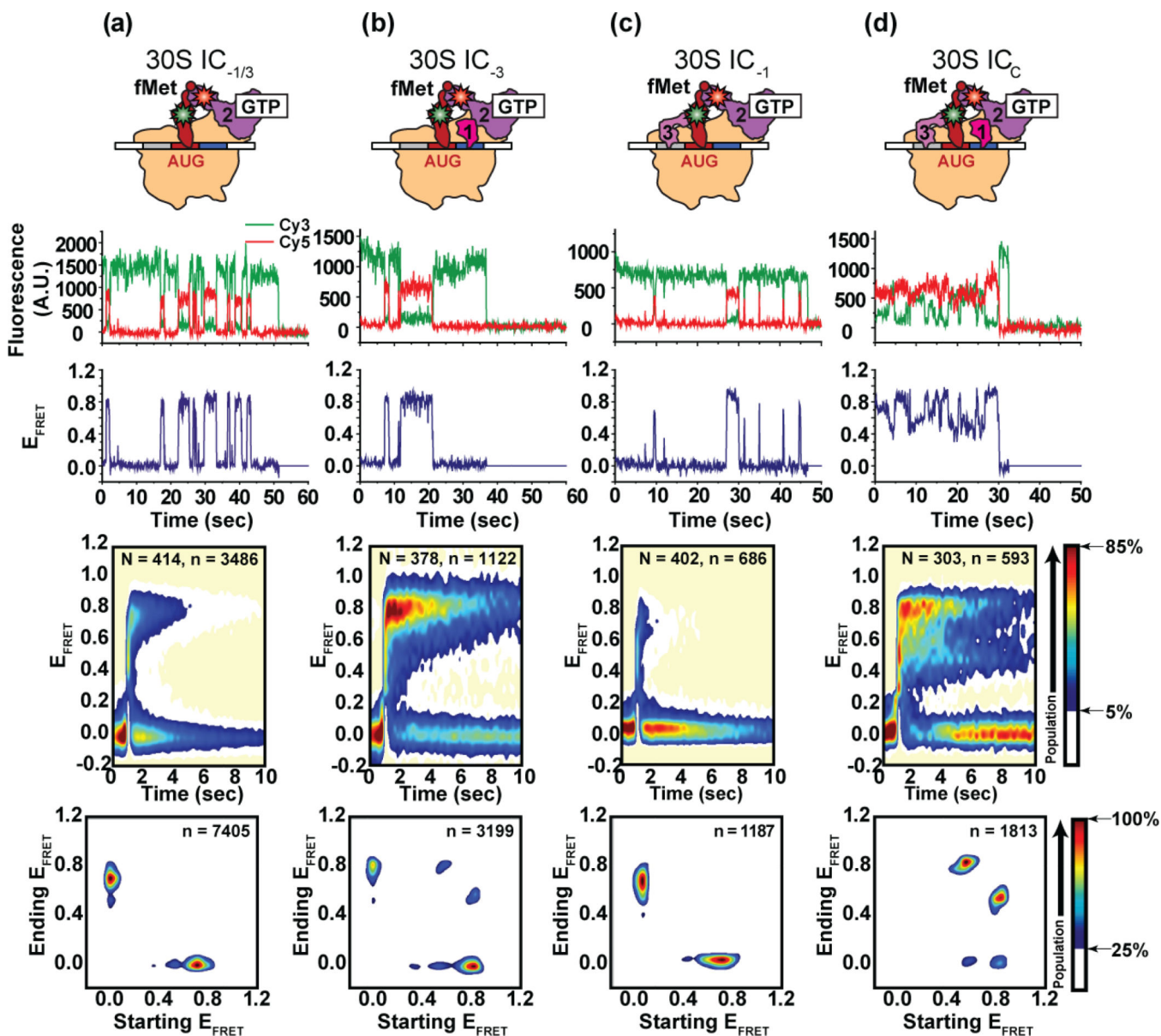


**Figure 2.**

The effect of IF1 and IF3 on the stability of IF2 and the conformational dynamics of the IF2•tRNA sub-complex. Cartoon representations of each of the 30S ICs investigated are shown along the top row. In each case, the IF2-bound state of the 30S IC is depicted. Representative Cy3 (green) and Cy5 (red) emission intensities *versus* time trajectories are shown in the second row, and the corresponding  $E_{\text{FRET}}$  *versus* time trajectories are shown in the third row. Binding of IF2 results in an increase Cy5 intensity and an anti-correlated decrease in Cy3 intensity due to FRET. Accordingly, the IF2-bound state of the 30S IC corresponds to the non-zero portions of the  $E_{\text{FRET}}$  *versus* time trajectories. Post-synchronized surface contour plots of the time evolution of population FRET are shown in the fourth row. Surface contour plots were generated as described in the Results and in Supplementary Fig. 5d. “N” indicates the total number of  $E_{\text{FRET}}$  *versus* time trajectories for each 30S IC and “n”

indicates the total number of individual IF2 binding events. The surface contours were plotted from tan (lowest population plotted) to red (highest population plotted) as indicated in the population color bar. Transition density plots (TDPs) are shown in the fifth row. TDPs were generated by plotting the “Starting  $E_{\text{FRET}}$ ” versus the “Ending  $E_{\text{FRET}}$ ” for each transition identified in the idealized  $E_{\text{FRET}}$  trajectories as a surface contour plot of a two-dimensional  $E_{\text{FRET}}$  histogram as described in Supplementary Fig. 5e. “n” indicates the total number of transitions that were used to generate each TDP. Surface contours are plotted from tan (lowest population plotted) to red (highest population plotted) as indicated in the population color bar. **(a)** 30S IC<sub>-1/3</sub>, **(b)** 30S IC<sub>-3</sub>, **(c)** 30S IC<sub>-1</sub>, and **(d)** 30S IC<sub>C</sub>.



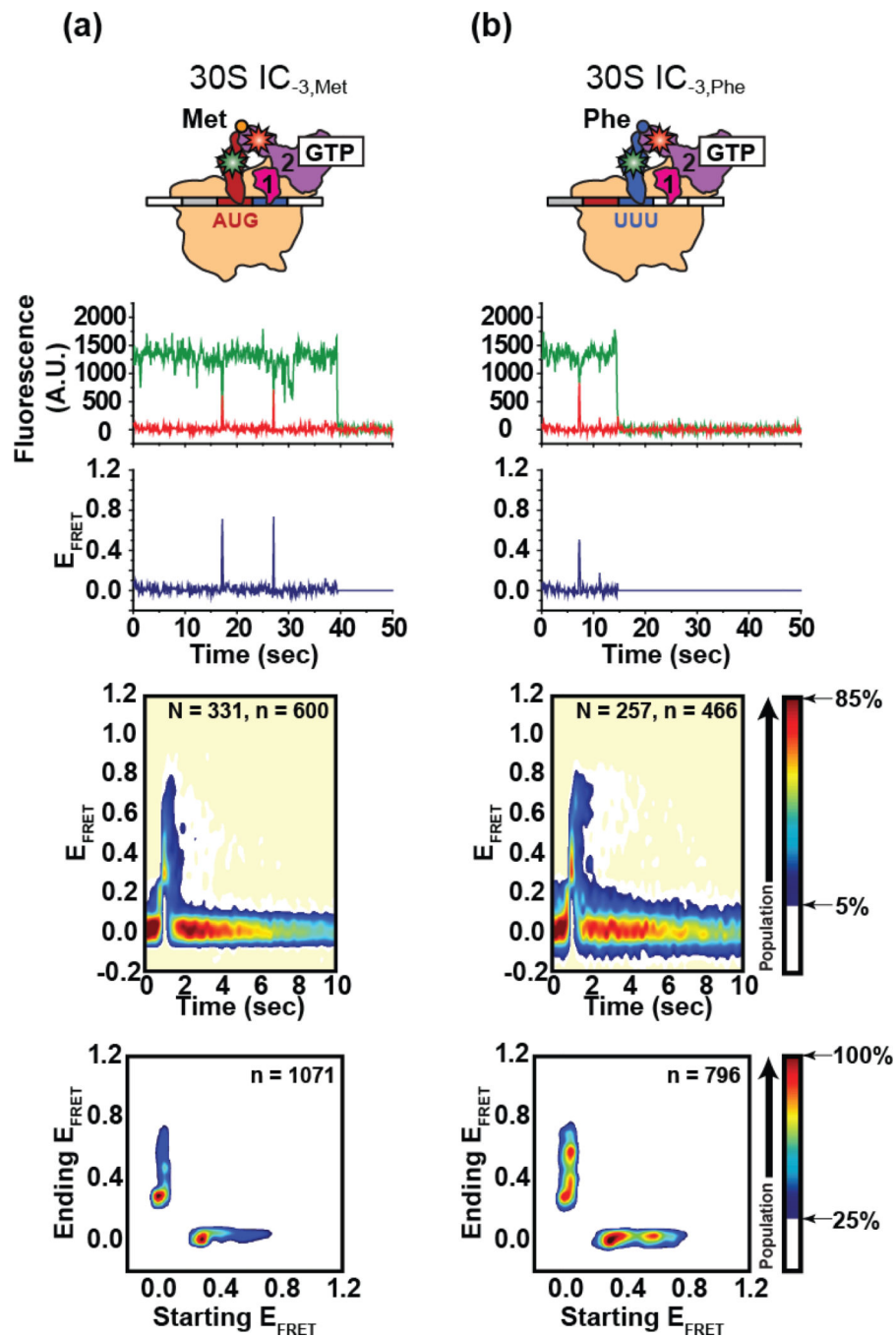


**Figure 3.** The effect of the P-site tRNA on the stability of IF2 and the conformational dynamics of the IF2•tRNA sub-complex. The layout of rows in this figure is identical to that in Fig 2. (a) 30S IC<sub>-3, Met</sub> and (b) 30S IC<sub>-3, Phe</sub>.

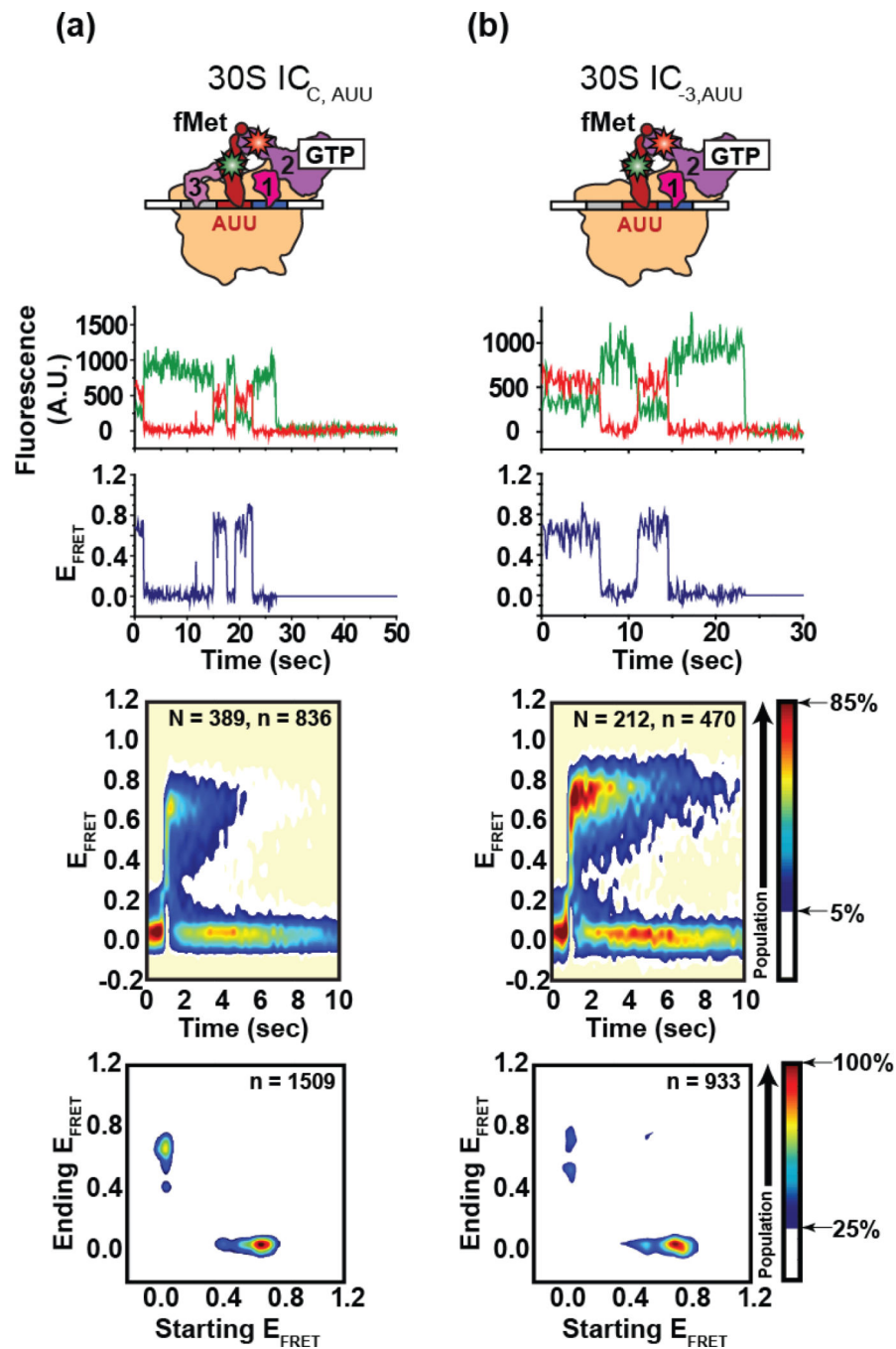


**Figure 4.** The effect of the P-site codon on the stability of IF2 and the conformational dynamics of the IF2•tRNA sub-complex. The layout of rows in this figure is identical to that in Fig 2. (a) 30S IC<sub>C, AUU</sub> and (b) 30S IC<sub>-3, AUU</sub>

**Table 1**

The association rate constant ( $k_{a,app}$ ), dissociation rate constant ( $k_{d,app}$ ), and dissociation equilibrium constant ( $K_{d,app}$ ) for the interaction of IF2 with each of various 30S ICs carrying different combinations of IFs, tRNAs, and start codons.

Complex	$k_{a,app}$ ( $\mu\text{M}^{-1} \text{s}^{-1}$ ) <sup>a</sup>	$k_{d,app}$ ( $\text{s}^{-1}$ ) <sup>a</sup>	$K_{d,app}$ (nM)
30S IC <sub>-1/3</sub>	13±1 <sup>b</sup>	0.6±0.2	50±20
30S IC <sub>-3</sub>	10±2 <sup>b</sup>	0.20±0.01	20±4
30S IC <sub>-1</sub>	3.32±0.03	2.1±0.3	600±100
30S IC <sub>C</sub>	8.9±0.7 <sup>c</sup>	0.013±0.002 <sup>d</sup>	1.6±0.3
30S IC <sub>C,Met</sub>	N.D. <sup>e</sup>	N.D.	N.D.
30S IC <sub>C,Phe</sub>	N.D.	N.D.	N.D.
30S IC <sub>-1/3,Met</sub>	0.019±0.002 <sup>f</sup>	1.3±0.3	70000±20000
30S IC <sub>-3,Met</sub>	0.29±0.02 <sup>f</sup>	1.5±0.1	5000±500
30S IC <sub>-3,Phe</sub>	0.18±0.01 <sup>f</sup>	1.3±0.2	7000±1000
30S IC <sub>-1/3,AUU</sub>	8.7±0.8	0.59±0.04	68±8
30S IC <sub>-3,AUU</sub>	5.5±0.2	0.35±0.02	63±4
30S IC <sub>-1,AUU</sub>	4.27±0.04	2.0±0.3	470±70
30S IC <sub>C,AUU</sub>	4.2±0.1	0.65±0.06	160±20

<sup>a</sup>  $k_{a,app}$  and  $k_{d,app}$  were determined using curve fitting-based population decay analyses as described in the Materials and Methods and in Supplementary Notes 3 and 4.

<sup>b</sup>  $k_{a,app}$  was determined from an experiment in which the rate of IF2 association was measured as a function of free IF2 concentration as described in the Results and Supplementary Fig. 6.

<sup>c</sup>  $k_{a,app}$  was determined from a pre-steady-state smFRET experiment as described in the Materials and Methods and Supplementary Notes 3 and 4.

<sup>d</sup>  $k_{d,app}$  was determined from an experiment performed with shuttering of the laser excitation source as described in the Materials and Methods and in Supplementary Notes 3 and 4.

<sup>e</sup> N.D. stands for “not detected”.

<sup>f</sup>  $k_{a,app}$  was obtained using a transition probability matrix-based population decay analysis as described in the Materials and Methods and in Supplementary Notes 3 and 4.

**Table 2**

Comparison of the ensemble rate of subunit joining reported in the literature and the occupancy of IF2 on the 30S IC estimated from the present work for various 30S ICs.

Complex	Rate of Subunit Joining (s <sup>-1</sup> ) <i>a,b</i>	IF2 Occupancy (%) <sup>c</sup>
30S IC <sub>-1/3</sub>	36 <sup>a</sup>	88
30S IC <sub>-3</sub>	42 <sup>a</sup>	94
30S IC <sub>-1</sub>	8.7 <sup>a</sup>	50
30S IC <sub>C</sub>	2.9 <sup>a</sup>	100
30S IC <sub>-1/3,Met</sub>	0.51 <sup>a</sup>	1.3
30S IC <sub>-3,Met</sub>	5.2 <sup>a</sup>	14
30S IC <sub>-3,Phe</sub>	4.0 <sup>a</sup>	11
30S IC <sub>C</sub>	5.4 <sup>b</sup>	98
30S IC <sub>C,AUU</sub>	0.06 <sup>b</sup>	50

<sup>a</sup>Rate of subunit joining reported by Antoun, *et al*<sup>10</sup>.

<sup>b</sup>Rate of subunit joining reported by Milon, *et al*<sup>14</sup>.

<sup>c</sup>IF2 occupancy = ([IF2/30S]/[30S]), where [IF2/30S] was calculated by applying the quadratic binding equation<sup>55</sup> to the apparent equilibrium dissociation constants reported in Table 1 and the concentrations of IF2 and 30S subunits used in the corresponding ensemble kinetic studies from which the subunit joining rates in column 2 of the present table were obtained.

Author Manuscript

Author Manuscript

Author Manuscript

Author Manuscript

**Table 3**

Comparison of the change in the rate of subunit joining calculated using ensemble rates of subunit joining reported in the literature with the change in the occupancy of IF2 on the 30S IC estimated from the present work for various pairs of 30S ICs. The two pairs of 30S ICs that exhibit the largest discrepancies in these two parameters are bolded and italicized.

Complexes	Change in the Rate of Subunit Joining <sup>a</sup>	Change in the IF2 Occupancy <sup>b</sup>
30S IC <sub>-3</sub> vs. 30S IC <sub>-1/3</sub>	1.2	1.1
30S IC <sub>-3</sub> vs. 30S IC <sub>-1</sub>	4.8	1.9
<b><i>30S IC<sub>C</sub> vs. 30S IC<sub>-3</sub></i></b>	<b><i>14.5</i></b>	<b><i>1.1</i></b>
30S IC <sub>-1/3</sub> vs. 30S IC <sub>-1/3,Met</sub>	72	68
30S IC <sub>-3</sub> vs. 30S IC <sub>-3,Met</sub>	8.1	6.7
30S IC <sub>-3</sub> vs. 30S IC <sub>-3,Phe</sub>	10.5	8.5
<b><i>30S IC<sub>C</sub> vs. 30S IC<sub>C,AUU</sub></i></b>	<b><i>90</i></b>	<b><i>2</i></b>

<sup>a</sup> Calculated using the rates of subunit joining reported in Table 2.

<sup>b</sup> Calculated using the IF2 occupancies reported in Table 2.